Geochemistry Geophysics Geosystems G3
AN ELECTRONIC JOURNAL OF THE EARTH SCIENCES
Published by AGU and the Geochemical Society

Article
Volume 9, Number 12
18 December 2008
Q12022, doi:10.1029/2008GC002107
ISSN: 1525-2027

Upper mantle seismic structure beneath the Ethiopian hot spot: Rifting at the edge of the African low-velocity anomaly

I. D. Bastow
Department of Earth Sciences, University of Bristol, Bristol BS8 1RJ, UK (ian.bastow@bristol.ac.uk)

A. A. Nyblade
Department of Geosciences, Pennsylvania State University, University Park, Pennsylvania 16802, USA

G. W. Stuart
School of Earth and the Environment, University of Leeds, Leeds LS2 9JT, UK

T. O. Rooney
Department of Geological Sciences, Michigan State University, East Lansing, Michigan 48824, USA

M. H. Benoit
College of New Jersey, Science Complex P-113, Ewing, New Jersey 08628, USA

[1] The Miocene-Recent East African Rift in Ethiopia subaerially exposes the transitional stage of rifting within a young continental flood basalt province. As such, it is an ideal study locale for continental breakup processes and hot spot tectonism. We combine teleseismic traveltime data from 108 seismic stations deployed during two spatially and temporally overlapping broadband networks to present detailed tomographic images of upper mantle *P* and *S* wave seismic velocity structure beneath Ethiopia. Tomographic images reveal a ~500 km wide low *P* and *S* wave velocity zone at 75 to ≥400 km depth in the upper mantle that extends from close to the eastern edge of the Main Ethiopian Rift (MER) westward beneath the uplifted and flood basalt-capped NW Plateau. We interpret this broad low-velocity region (LVR) as the upper mantle continuation of the African Superplume. Within the broad LVR, zones of particularly low velocity are observed with absolute delay times ($\delta t_P \sim 4$ s) that indicate the mantle beneath this region is amongst the slowest worldwide. We interpret these low velocities as evidence for partial melt beneath the MER and adjacent NW Plateau. Surprisingly, the lowest-velocity region is not beneath Afar but beneath the central part of the study area at ~9°N, 39°E. Whether this intense low-velocity zone is the result of focused mantle upwelling and/or enhanced decompressional melting at this latitude is unclear. The MER is located toward the eastern edge of the broad low-velocity structure, not above its center. This observation, along with strong correlations between low-velocity zones and lithospheric structures, suggests that preexisting structural trends and Miocene-to-Recent rift tectonics play an important role in melt migration at the base of the lithosphere in this magmatic rift zone.

Components: 5615 words, 9 figures.

Keywords: seismology; rift; lithosphere; Africa; mantle.

Index Terms: 7203 Seismology: Body waves; 7208 Seismology: Mantle (1212, 1213, 8124); 7270 Seismology: Tomography (6982, 8180).

Received 22 May 2008; **Revised** 3 September 2008; **Accepted** 28 October 2008; **Published** 18 December 2008.

Bastow, I. D., A. A. Nyblade, G. W. Stuart, T. O. Rooney, and M. H. Benoit (2008), Upper mantle seismic structure beneath the Ethiopian hot spot: Rifting at the edge of the African low-velocity anomaly, *Geochem. Geophys. Geosyst.*, *9*, Q12022, doi:10.1029/2008GC002107.

1. Introduction

1.1. Overview

[2] Ethiopia has long been recognized as an ideal location to study rifting and hot spot tectonism because of the Cenozoic continental flood basalt volcanism, plateau uplift, and transition from continental rifting to incipient seafloor spreading found there [*Ebinger and Casey*, 2001; *Nyblade and Langston*, 2002; *Furman et al.*, 2006]. In this paper, we use new *P* and *S* wave tomographic models of upper mantle structure beneath Ethiopia to advance our understanding of the origin, nature, and evolution of the Ethiopian hot spot and the Main Ethiopian Rift (MER).

[3] Many authors have invoked starting thermal plumes [*Griffiths and Campbell*, 1990], citing surface observations such as geochemistry and elevated topography, to explain Ethiopia's hot spot tectonism, but the location and number of plumes or upper mantle convective cells is often debated [e.g., *Schilling et al.*, 1992; *Burke*, 1996; *Ebinger and Sleep*, 1998; *George et al.*, 1998; *Courtillot et al.*, 1999; *Rogers et al.*, 2000; *Furman et al.*, 2006; *Rogers*, 2006]. For example, *Ebinger and Sleep* [1998] suggested that one large plume spread beneath the African Plate near Turkana at ~45 Ma but only small amounts of melt volume were produced until lithospheric thinning commenced in the Red Sea and Gulf of Aden. Topography at the base of the lithosphere channeled buoyant material up to ~1000 km from Turkana to the evolving Red Sea rift and the Mesozoic rift zones of eastern and central Africa. Alternatively, *George et al.* [1998] and *Rogers et al.* [2000] cite differences in geochemistry between Afar and Kenya to propose that two Cenozoic plumes may have existed, one rising and dispersing beneath southern Ethiopia at ~45 Ma and the other rising beneath the Afar depression. *Furman et al.* [2006] modify the single plume hypothesis to invoke ideas of multiple plume stems rising from a long-lived deeper feature of the mantle (the African Superplume). *Kieffer et al.* [2004] claim that Oligocene Ethiopian Plateau volcanism was sourced from a broad region of hot, heterogeneous mantle, with little or no input from the lithospheric mantle. Plume models have also been advocated in many other related studies, for instance, *Schilling et al.* [1992], *Baker et al.* [1996], *Burke* [1996], *Courtillot et al.* [1999], *Pik et al.* [1999], *Rogers* [2006], *Pik et al.* [2006].

[4] Within the context of the plume model, the roles of lithospheric structure and process have also been called upon to explain complexities in plateau volcanism [e.g., *Furman et al.*, 2006; *Furman*, 2007], uplift [e.g., *Gani et al.*, 2007], and MER evolution [e.g., *Rooney et al.*, 2005; *Bastow et al.*, 2005; *Yirgu et al.*, 2006; *Keranen and Klemperer*, 2007; *Rooney et al.*, 2007; *Corti*, 2008]. However, even though lithospheric structural inheritance can strongly influence continental rift development, [e.g., *Vauchez et al.*, 1997], the nature of plume-lithosphere interactions remains poorly understood outside a 250 × 350 km area centered on the MER [*Bastow et al.*, 2005]. Beneath the MER a relatively narrow (~75 km wide) low-velocity zone was noted at lithospheric depths. *Benoit et al.* [2006b] suggested a westward dip to Ethiopia's broad (≥500 km wide) upper mantle low-velocity region (LVR), implying that the MER may not have formed directly above the mantle upwelling. However, their study lacked resolution above 150 km and so the extent to which the MER and flood basaltic magmatism may have formed in an asymmetric manner with respect to the underlying mantle is not known.

[5] Looking deeper into the mantle, recent seismic studies suggest that the hot spot activity in Ethiopia and surrounding regions may be linked to the African Superplume, a broad (~500 km wide) ~3% *S* wave slow-velocity anomaly that originates at the core-mantle boundary beneath southern Africa and rises toward the base of the lithosphere somewhere in the region of Ethiopia and the Red Sea/Gulf of Aden [*Grand*, 2002; *Ritsema and Allen*, 2003; *Simmons et al.*, 2007; *Li et al.*, 2008]. When reviewed in light of other geophysical observations that can be used to constrain mantle convection (e.g., the global free-air gravity field, tectonic plate motions, and dynamic surface

topography) the morphology and sharp velocity gradients of the African Superplume are explained best by a thermochemical plume rising from the core-mantle boundary [e.g., *Ni et al.*, 2002; *Simmons et al.*, 2007]. Precisely where or how the superplume crosses the transition zone remains unclear [e.g., *Nyblade et al.*, 2000; *Benoit et al.*, 2003, 2006a]. There is, however, increasing evidence from global tomographic studies that low-velocity structures could be continuous across the 410 and 660 km discontinuities in the Kenya-Ethiopia region [e.g., *Ritsema and Allen*, 2003; *Li et al.*, 2008; *Montelli et al.*, 2004, 2006, and references therein]. Regional-scale surface wave studies [e.g., *Debayle et al.*, 2001] also provide evidence for a broad LVR throughout the Ethiopian upper mantle. Such deep mantle structures cannot easily be attributed to small-scale convection processes, which have also been proposed as alternatives to plumes in some large igneous provinces [e.g., *King and Ritsema*, 2000]. *Benoit et al.* [2006a, 2006b] noted that the upper mantle LVR is most pronounced beneath the MER, not the Afar. In contrast, global tomographic models [e.g., *Ritsema and Allen*, 2003; *Montelli et al.*, 2004, 2006; *Li et al.*, 2008] indicate that the lowest velocities lie beneath the Afar, consistent with many models for rifting and hot spot tectonism [*George et al.*, 1998; *Rogers et al.*, 2000; *Rogers*, 2006].

[6] To address outstanding questions about the origin and evolution of the Ethiopian hot spot and MER, here we combine broadband seismic data from the Ethiopian Broadband Seismic Experiment [*Nyblade and Langston*, 2002], the Ethiopia Afar Geoscientific Lithospheric Experiment (EAGLE) [*Bastow et al.*, 2005], and two permanent GDSN stations (ATD and FURI; Figure 1) to constrain Ethiopian upper mantle seismic structure. By combining data from two regional seismic experiments that targeted different parts of Ethiopia's upper mantle, we are able to image more clearly details of upper mantle seismic structure across the area than was previously possible. Our results provide new insights into the locus of mantle upwelling beneath the Ethiopian hot spot and the spatial and temporal development of the MER with respect to the underlying mantle structure.

1.2. Tectonic Setting

[7] The earliest Cenozoic volcanism in East Africa occurred in SW Ethiopia and the Turkana depression in northernmost Kenya at 40–45 Ma [e.g., *Ebinger et al.*, 1993; *George et al.*, 1998; *Furman et al.*, 2006]. Approximately 2 km of basalts and subordinate rhyolites were then erupted rapidly across the Ethiopian Plateau at ~29–31 Ma [*Mohr*, 1983; *Hofmann et al.*, 1997] prior to or concomitant with the onset of rifting in the Red Sea and Gulf of Aden [e.g., *Wolfenden et al.*, 2004]. Additional isolated shield volcanism in the interval ~30–10 Ma occurred across the Ethiopian Plateau (Figure 1) and added ~2 km of additional local relief in areas such as the Simien, Choke, and Guguftu shield volcanoes [e.g., *Kieffer et al.* 2004, Figure 1].

[8] The timing of uplift in Ethiopia is controversial; commencement has been estimated at 20–30 Ma on the basis of U-Th/He thermochronometry data [*Pik et al.*, 2003], but more recent studies indicate an episodic uplift history with ~1 km uplift being produced more recently (~10 Ma to the present), postulated to be due to foundering of the Plateau lithosphere following extensive heating and weakening since the onset of flood basalt volcanism at ~30 Ma [*Gani et al.*, 2007].

[9] The Miocene-Recent MER forms the third arm of the Red Sea, Gulf of Aden rift-rift-rift triple junction where the Arabian, Nubian, Somalian and Danakil Plates meet in Afar [e.g., *Wolfenden et al.* 2004]. The MER formed within the Precambrian metamorphic crustal basement of the Pan-African Mozambique belt [*Kazmin et al.*, 1978] that exhibits N-S to NNE-SSW suture zones [*Vail*, 1983; *Berhe*, 1990] and NW-SE oriented strike-slip faults [*Brown*, 1970; *Purcell*, 1976]. Extension in SW Ethiopia and the Turkana Depression in northern Kenya commenced by ~20 Ma with central and northern sectors of the MER developing between 18 and 10 Ma, respectively [e.g., *WoldeGabriel*, 1988; *Wolfenden et al.*, 2004]. Large offset border faults formed along one or both sides of the rift (Figure 1) and are often marked by chains of silicic centers [e.g., *Chernet et al.*, 1998]. South of ~7.5°N, a broad (~500 km wide) faulted region extends to the west of the present day MER and marks the zone across which the MER has migrated east since Oligocene times [e.g., *Ebinger et al.*, 2000].

[10] *Wolfenden et al.* [2004] suggest that deformation in the MER north of 8.5°N migrated to the center of the rift some time in the interval 6.6–3 Ma, with an associated change from 130°E directed extension to 105°E directed extension. Geodetic data indicate that the MER is currently extending in a direction N94°E at 7 mm a^{-1} [*Fernandes et al.*, 2004] and it has been proposed

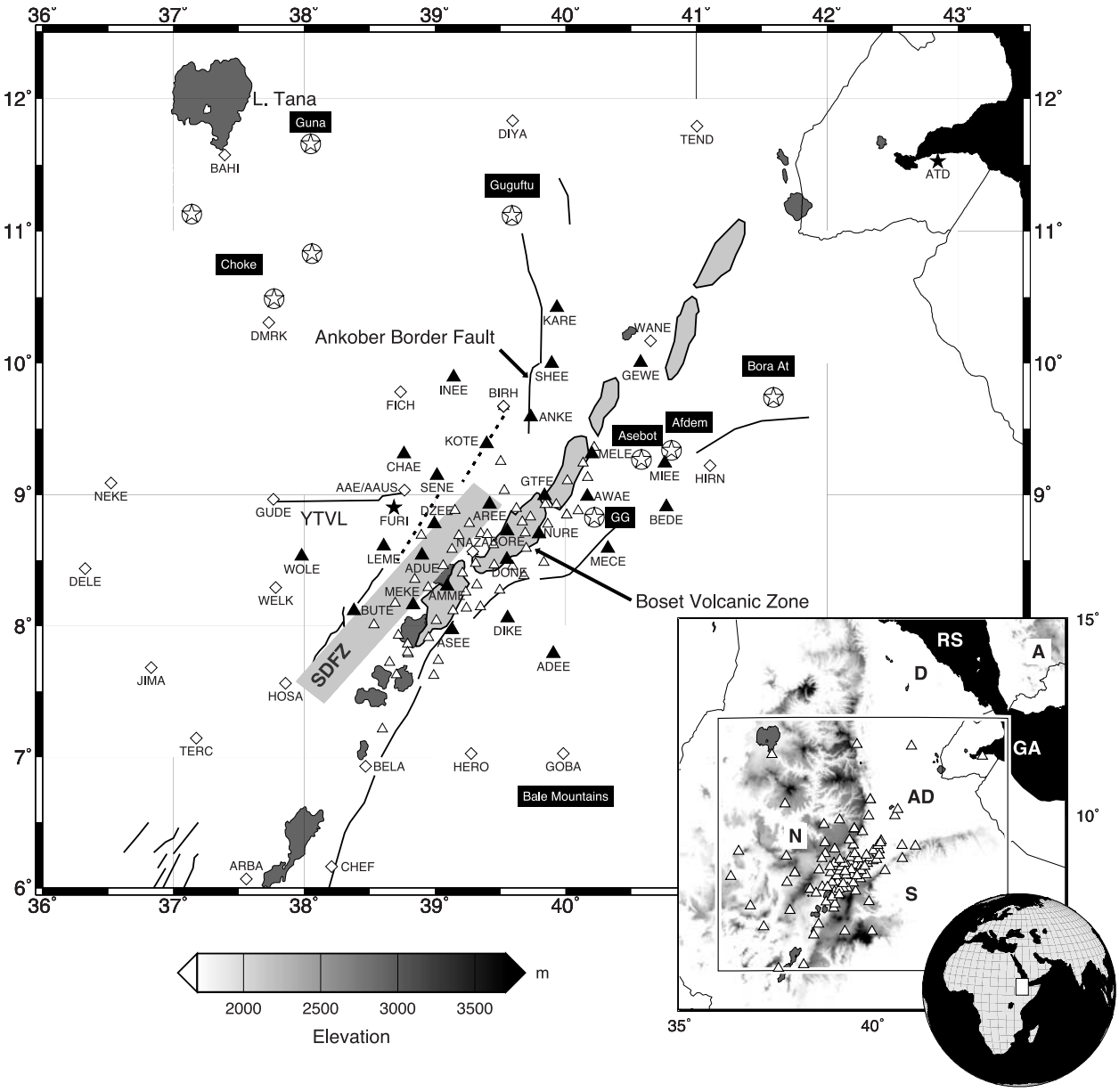

Figure 1. The location of the passive network stations. Filled triangles are the EAGLE Phase I passive experiment stations (October 2001 to January 2003). Open triangles are the EAGLE Phase II passive experiment stations (November 2002 to February 2003). Open diamonds are Penn State Ethiopia passive experiment stations (March 2000 to March 2002). Permanent stations FURI and ATD are shown by the black stars. Major mid-Miocene border faults and Quaternary magmatic zones along the Wonji Fault Belt (WFB) are shown by the heavy black lines; dashed lines are faulted monoclines. Circled stars are selected 30 Ma to recent volcanoes; GG is Gara Gumbi. SDZF is the Silti Debre Zeyit Fault Zone. YTVL is the Yerer Tullu Wellel Volcanic Zone. Inset shows the regional tectonic setting on a topographic map. RS, Red Sea; GA, Gulf of Aden; A, Arabian Plate; AD, Afar Depression; D, Danakil Microplate; N, Nubian Plate; S, Somalian Plate. Open triangles are the locations of all broadband stations used in this study.

that ~80% of the present-day strain is localized within the MER [*Bilham et al.*, 1999]. On the strength of this evidence, *Ebinger and Casey* [2001] proposed that the locus of extension in this transitional rifting environment has localized progressively since ~12 Ma, away from the mid-Miocene border faults, toward en echelon chains of eruptive magmatic centers, dykes, and small offset faults. Thus magmatic emplacement, not border faulting, increasingly dominates the rifting

process after the initial stages of breakup [e.g., *Ebinger and Casey*, 2001; *Keranen et al.*, 2004; *Rooney et al.*, 2005; *Keranen and Klemperer*, 2007].

[11] Much of the Quaternary magmatic activity within the MER has occurred in magmatic zones in the center of the rift north of 8.5°N in the Wonji Fault Belt (WFB) [e.g., *Mohr*, 1967; *Ebinger and Casey*, 2001] where magmas fractionate at shallow (<5 km) depths [*Rooney et al.*, 2007]. South of 8.5°N, the WFB is offset within the MER toward the Somalian Plate and is flanked to the west by the Silti Debre Zeyit Fault Zone (SDFZ, Figure 1), in which magmas fractionate at various depths throughout the crust [*Rooney et al.*, 2005, 2007]. *Rooney et al.* [2007] cite these differences in magmatic plumbing system north and south of ~8.5°, in conjunction with local seismicity [*Keir et al.*, 2006] and magnetotelluric results [*Whaler and Hautot*, 2006] to suggest that a simple south-to-north transition from continental rifting to seafloor spreading may be inappropriate and that the MER has formed as a result of the southward propagation of the Red Sea Rift and northward propagation of the East African Rift, merging at 8.5°N. Magmatic processes in the Afar Depression and MER continue to the present day in this active magmatic rift zone [e.g., *Tadesse et al.*, 2003; *Wright et al.*, 2006].

2. Method

2.1. Data

[12] Broadband recordings of teleseismic *P* and *S* wave traveltime data from two major seismic experiments in Ethiopia have been combined in the present study. Twenty seven broadband seismometers operated between March 2000 and March 2002 as part of the Ethiopia Broadband Seismic Experiment [*Nyblade and Langston*, 2002] that covered an area ~650 × 750 km, with station spacing ~100 km to give broad spatial coverage over the uplifted Ethiopian Plateau (Figure 1). Spatially and temporally overlapping with this experiment, the 29 broadband seismometers of the EAGLE broadband network [*Bastow et al.*, 2005] recorded between October 2001 and January 2003 over an area 250 × 350 km centered on the Boset volcanic zone in the center of the rift (Figure 1). Six of the EAGLE seismometers were colocated with Ethiopia Broadband Seismic Experiment instruments. These stations were spaced at ~40 km and were designed to probe lithospheric seismic structure. Fifty CMG-6TD instruments that recorded between November 2002 and February 2003 during the EAGLE phase II Rift Valley Experiment [*Keir et al.*, 2006] complete our telescoping view of Ethiopian seismic structure. Permanent IRIS GSN/GDSN stations FURI and ATD were also operational throughout all temporary network deployments.

[13] For the ~3 year period for which we have data, waveforms from ~1000 earthquakes of magnitude mb $\geq$ 5.5 in the teleseismic epicentral distance (Δ) range 30°< Δ < 103° were visually inspected for those with good signal-to-noise ratio on at least 10 stations. For *P* waves we finally analyzed the recordings from 191 teleseismic earthquakes together with 11 earthquakes that were at distances (Δ > 103°) from which core (*PKP*) phases were recorded. Further visual inspection of 1000 lower magnitude earthquakes (4.4 < mb < 5.5) yielded an additional 25 earthquakes to improve the uniformity of data coverage with respect to back azimuth and epicentral distance. *S* wave arrivals were inspected in a similar manner to yield a database of 40 *S* wave and 70 *SKS* phase earthquakes. Figure 2 shows the relatively uniform distribution of these earthquakes with respect to the center of the study area.

2.2. Method of Relative Arrival Time Determination

[14] Manual picking of the first arriving *P* wave identifiable across the network was performed on waveforms that were filtered with a zero-phase two-pole Butterworth filter with corner frequencies of 0.4–2 Hz. Direct *S* waves were picked similarly on transverse component seismograms to minimize contamination by *P* and *P* to *S* wave converted phases and were filtered between 0.04 and 0.15 Hz. *SKS* phases were picked on radial component seismograms. Subsequently, phase arrivals and relative arrival time residuals were more accurately determined using the multichannel cross-correlation technique (MCCC) of *VanDecar and Crosson* [1990]; we selected a window (3 s for *P* waves and 12 s for *S* waves) containing the initial phase arrival and typically one or two cycles of *P* or *S* wave energy to cross-correlate. Our chosen bandwidths are similar to those used in other teleseismic tomographic studies, but our low-pass levels of 2 Hz and 0.15 Hz for *P* and *S* waves, respectively, are higher than previous studies in Ethiopia (1 Hz for *P* waves [*Benoit et al.*, 2006b]; 0.1 Hz for *S* waves [*Bastow et al.*, 2005; *Benoit et al.*, 2006a,

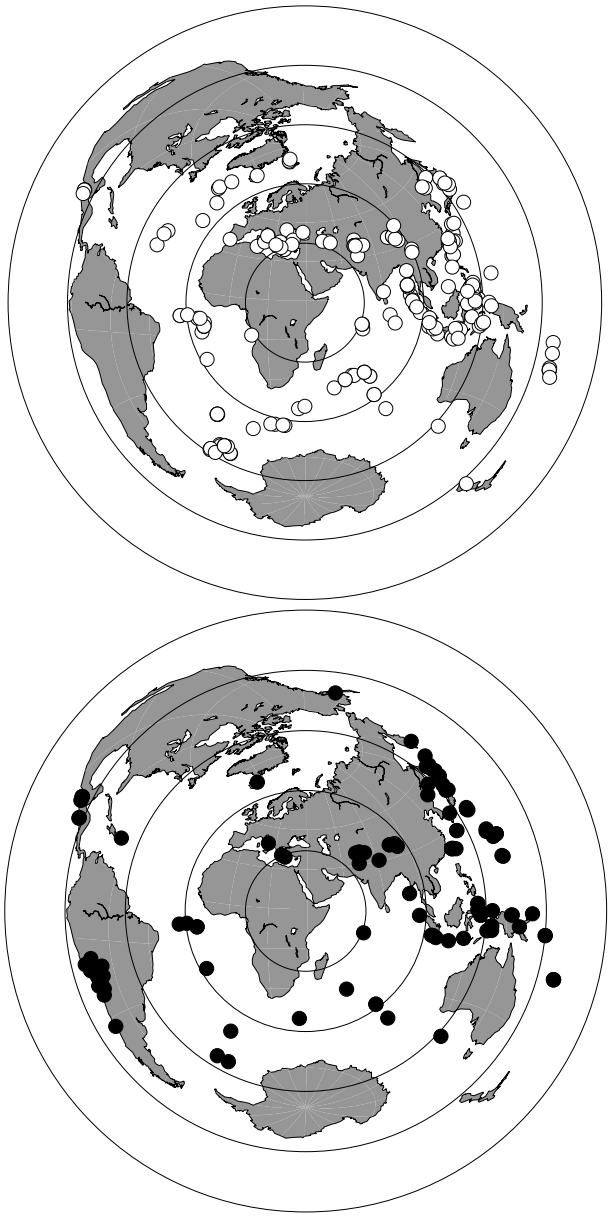

Figure 2. Back azimuth and distance distribution of earthquakes for (top) *P* waves and (bottom) *S* waves used in this study. The concentric circles on the plot indicate 30° intervals from the center of the network at 9°N, 39°E.

2006b]). Filter bandwidths are designed to retain as high a frequency as possible since our inversion procedure adopts ray theory (the infinite frequency approximation). We eliminate all waveforms with cross-correlation coefficients <0.85 from our analysis.

[15] The MCCC method also provides a means of quantifying the standard error associated with each arrival time. In this study relative arrival times determined in this way have mean standard deviation 0.02 s, and 0.05 s for *P* and *S* waves, respectively. In line with the studies of *Bastow et al.* [2005] and *Tilmann et al.* [2001] we regard the MCCC derived estimates of timing uncertainty as optimistic.

[16] Relative arrival time residuals t_{RES} for each station are given by:

$$t_{RES_i} = t_i - (t_{e_i} - \overline{t_e}), \quad (1)$$

where t_i is the relative arrival time for each station i, t_{e_i} is the expected traveltime based on the IASP91 traveltime tables [*Kennett and Engdahl*, 1991] for the ith station, and $\overline{t_e}$ is the mean of the IASP91 predicted traveltimes associated with that particular event. Our final traveltime data sets comprise 4735 *P* traveltimes and 1634 *S* traveltimes.

2.3. Analysis of Traveltime Residuals

[17] *Bastow* [2005] analyzed International Seismological Catalogue (ISC) traveltime data for permanent station AAE (Figure 1) in Addis Ababa and showed that the mean absolute delay time with respect to the IASP91 traveltime tables for *P* waves arriving at AAE is +4.6 ± 0.15 s (2× standard error); the mantle beneath AAE is therefore amongst the slowest worldwide [see *Poupinet*, 1979]. The mean relative arrival time residual (equation (1)) for the temporary station in Addis Ababa (AAUS, Figure 1) is 0.08 s so we can consider our relative arrival time residuals in Ethiopia to be on a pedestal of ~4.1 s relative to the global average (after correction for elevation). If we assume that this delay in absolute *P* wave traveltimes occurs in the top 600 km of the mantle, all negative *P* wave velocity anomalies shown in our tomographic images (Figures 7, 8, and 9) could be considered ≥6% slow compared to normal mantle.

[18] Figure 3 shows plots of *P* and *S* wave relative arrival time residuals as a function of back azimuth and epicentral distance for stations ADEE and DIKE on the Somalian Plate; AREE, ASEE, and GEWE in the MER; BAHI and SENE on the NW Plateau (Figure 1). These data have been corrected for the effects of topography using correction velocities of 3 kms^{-1} and 1.7 kms^{-1} for *P* and *S* waves, respectively. Relative arrival time residuals vary smoothly as a function of back azimuth and epicentral distance at stations ASEE, AWAE, BIRH, BUTE, KARE, NAZA, and WOLE (Figure 1) that were occupied by both the EAGLE and Ethiopia

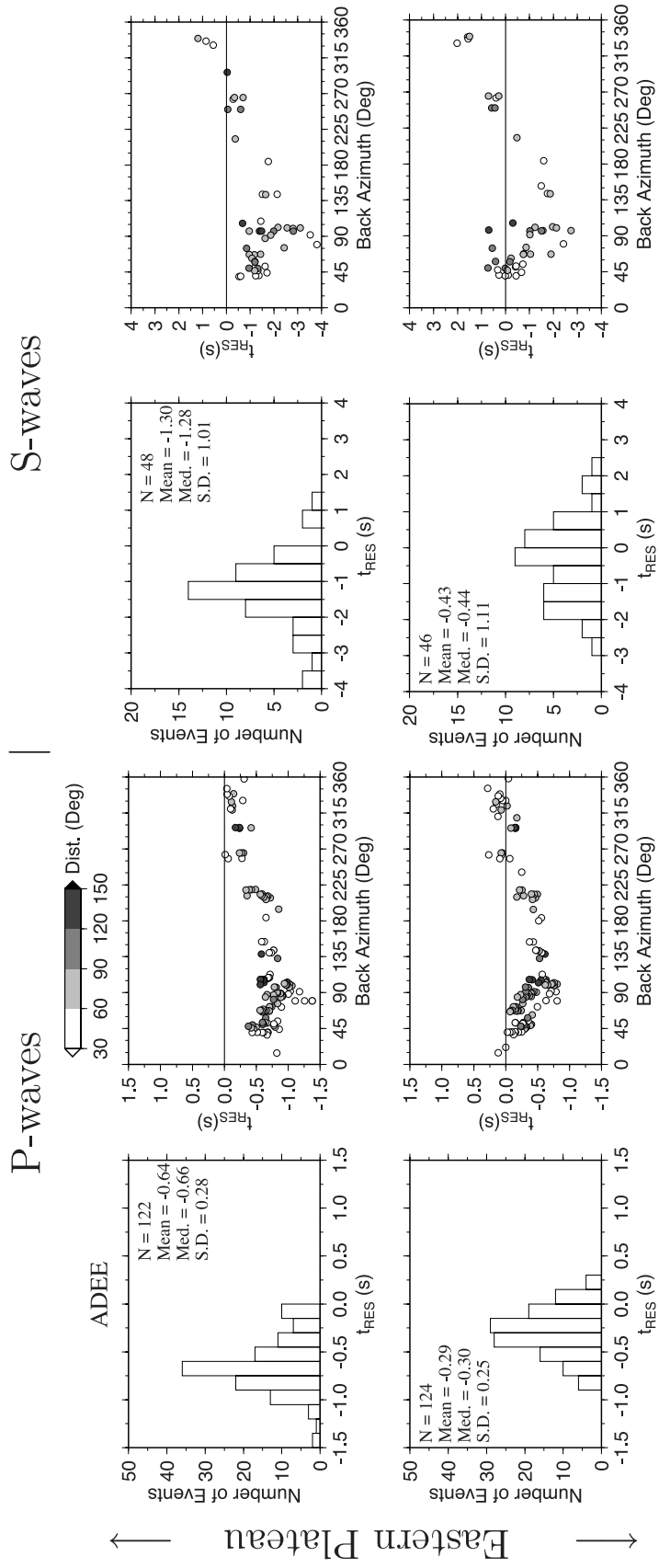

Figure 3. Variation of relative arrival time residuals for (left) *P* waves and (right) *S* waves as a function of back azimuth and epicentral distance. Negative arrival times indicate a relatively early arrival. Positive arrival times indicate a relatively late arrival.

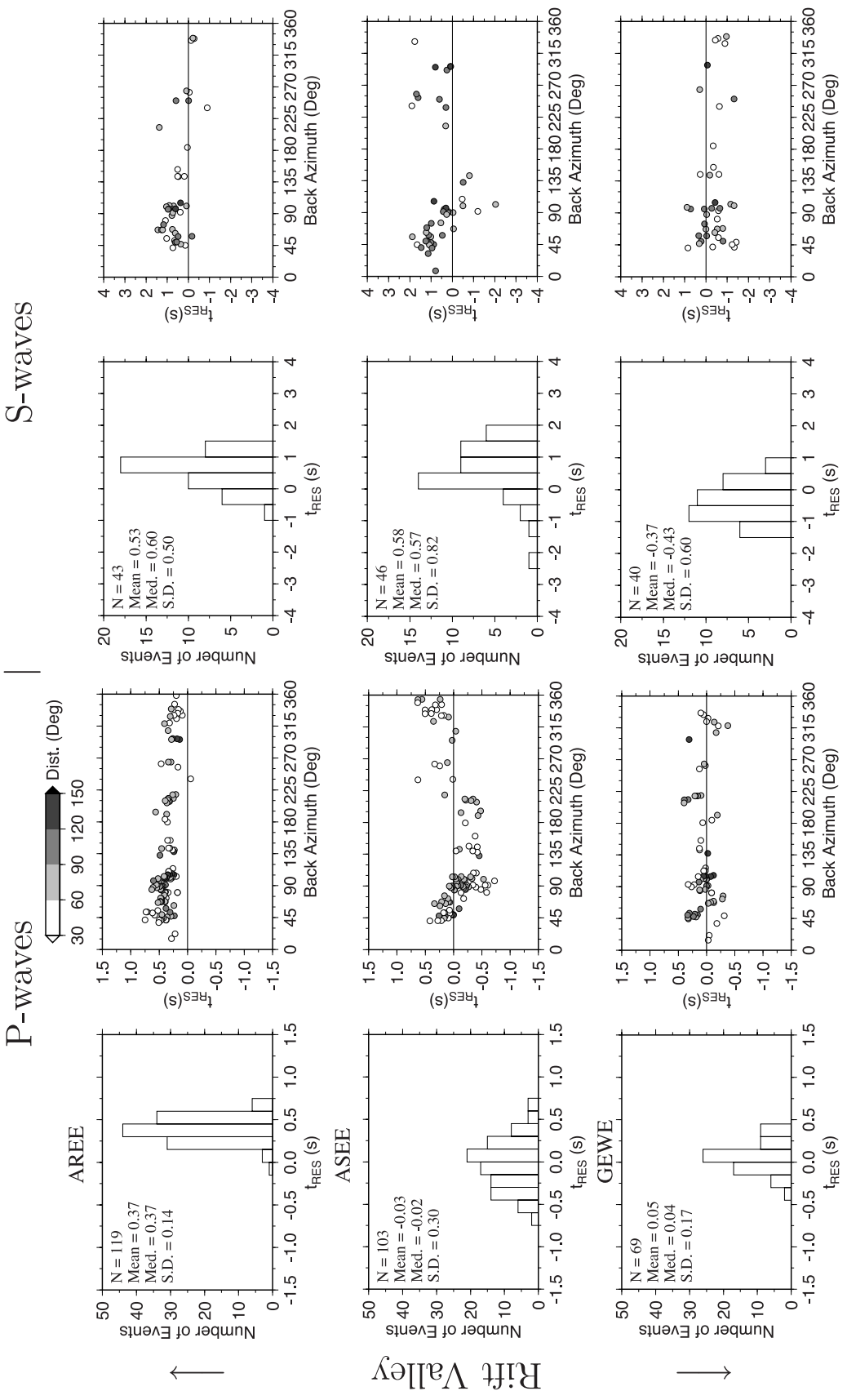

Figure 3. (continued)

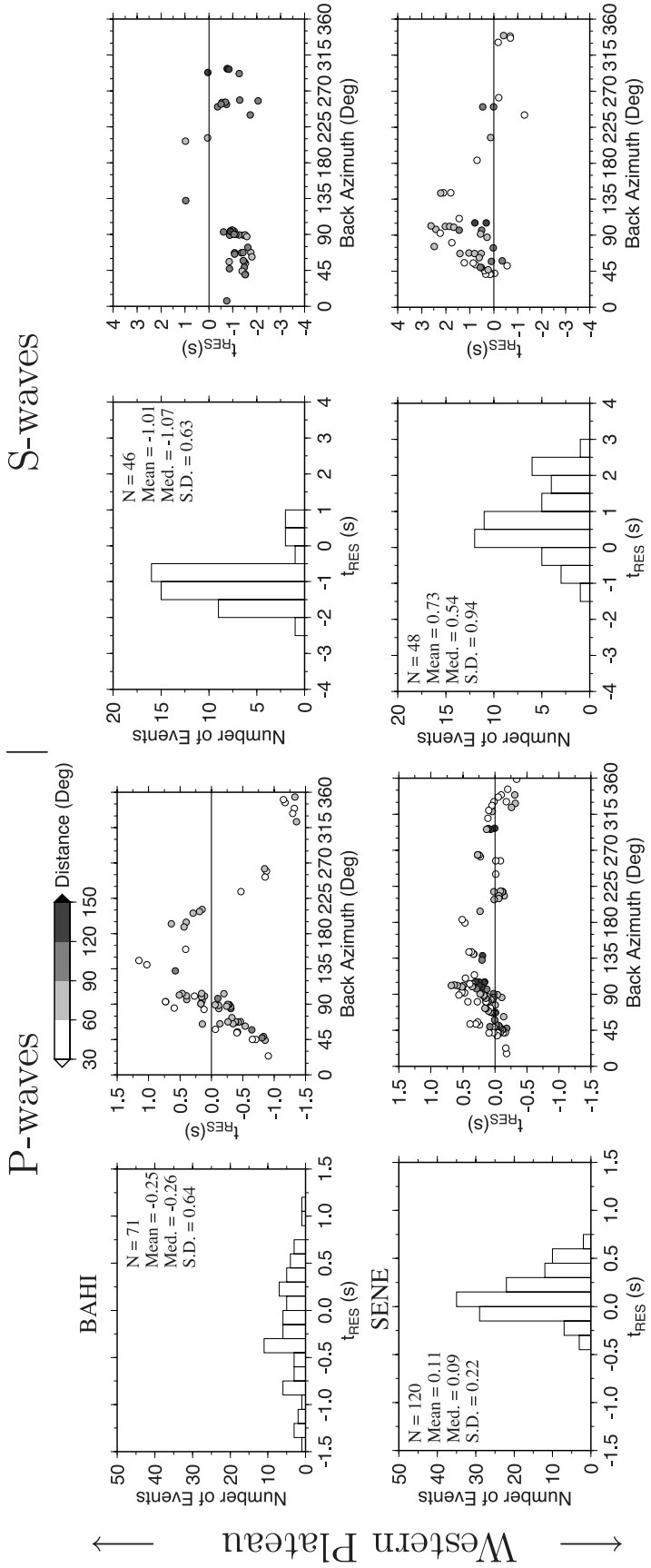

Figure 3. (continued)

Broadband Seismic Experiment networks show no offset in traveltime data (e.g., ASEE; Figure 3). Hence we are confident that our spatially and temporally overlapping networks have been combined successfully.

[19] Figure 3 provides several first-order observations about velocity structure in Ethiopia. Stations on the NW Plateau (e.g., SENE, BAHI) have relatively late arrivals from easterly and southerly back azimuths; rays traverse low-velocity structure beneath the rift. On the other hand, late arrivals on the Somalian Plate (e.g., DIKE, ADEE) come from westerly back azimuths. In the *P* wave study, the largest peak-to-peak variations in δt_P ($\sim$2.5 s) are seen at station BAHI (Figures 1 and 3). Arrivals from back azimuths that traverse the rift valley are later than from the north. Near the rift flanks, the largest peak-to-peak variations in δt_P are $\leq$1.5 s (e.g., SENE, DIKE; Figures 1 and 3). This dramatic change in δt_P at the western edge of the network may indicate our proximity to the edge of the African Superplume though a larger aperture network would confirm this hypothesis more confidently. Large negative relative arrival time residuals at station BAHI are also seen at station ADEE (Figure 1) in the SE corner of the network, $\sim$100 km from the MER. Variations in δt_S at BAHI do not show such extreme variations, possibly implying a greater sensitivity of the *S* wave data set to near-rift low-velocity partial melt [e.g., *Hammond and Humphreys*, 2000]. The true peak-to-peak variations in δt_S could be larger, however, since our back azimuth coverage is not complete at BAHI in the range 135–180°.

[20] Intriguingly, the stations with the latest mean relative arrival time residuals (e.g., AREE; Figures 1 and 3) are in the center of the study area around 9°N, 38°E (Figure 4). This result would be counterintuitive on the basis of models for rifting that consider the MER as a south-north transition from continental rifting to incipient seafloor spreading with an associated increase in melt volume toward the Red Sea and Gulf of Aden. The observations may instead be supportive of recent geochemical studies that interpret the MER at $\sim$9°N as a junction between two rifts: the southward propagating Red Sea rift and the northward propagating East African Rift [*Rooney et al.*, 2007]. Lower velocities beneath the MER also contrast with global seismic studies (that lack our dense station coverage), which indicate lowest velocities beneath Afar [e.g., *Montelli et al.* 2006].

2.4. Model Parameterization and Inversion Procedure

[21] We adopt the method of *VanDecar et al.* [1995] to image upper mantle velocity heterogeneities using regularized, nonlinear, least squares inversion of Ethiopian relative arrival time residuals. We adopt the same inversion procedure as the recent regional tomographic studies of *Bastow et al.* [2005], *Benoit et al.* [2006a], and *Benoit et al.* [2006b] in Ethiopia so meaningful comparisons can be made with the existing velocity models.

[22] Our parameterization scheme consists of 24 knots in depth between 0 and 800 km, 48 knots in latitude between 0 and 19°N, and 50 knots in longitude between 29 and 50°E: a total of 57,600 knots parameterizing slowness. Knot spacing is 25 km in the innermost resolvable parts (4.5–13°N, 36–44°E, 0–400 km depth). Outside this region, knot spacing increases to 50 km between 400 and 700 km and then to 100 km to 800 km depth. Thus we are limiting our structural interpretations to features of spatial wavelength $\geq$50 km in the top 400 km of our model.

[23] We parameterize outside the area of interest so that we do not map unwarranted and spurious structure into the region where we will be making our structural interpretations: a minimum structure approach [*VanDecar et al.*, 1995]. We do not parameterize deeper than 800 km since synthetic tests indicate that structures in the upper 500 km, where we have a high density of crossing rays, can be successfully differentiated from the deeper unresolvable parts of the model. In the regularized nonlinear least squares inversion procedure, we solve simultaneously for slowness perturbations, source terms and station terms [*VanDecar et al.*, 1995]. The source terms are free parameters used in the inversion procedure to account for small variations in back azimuth and incidence angle caused by distant heterogeneities and source mislocations. The station terms account for traveltime anomalies associated with the region directly beneath the station where the lack of crossing rays prevents the resolution of crustal structure.

Figure 4. Map plot of mean relative arrival time residual data for (top) *P* waves and (bottom) *S* waves. Squares are stations with negative relative arrival time residuals (relatively fast). Circles are stations with positive relative arrival time residuals (relatively slow).

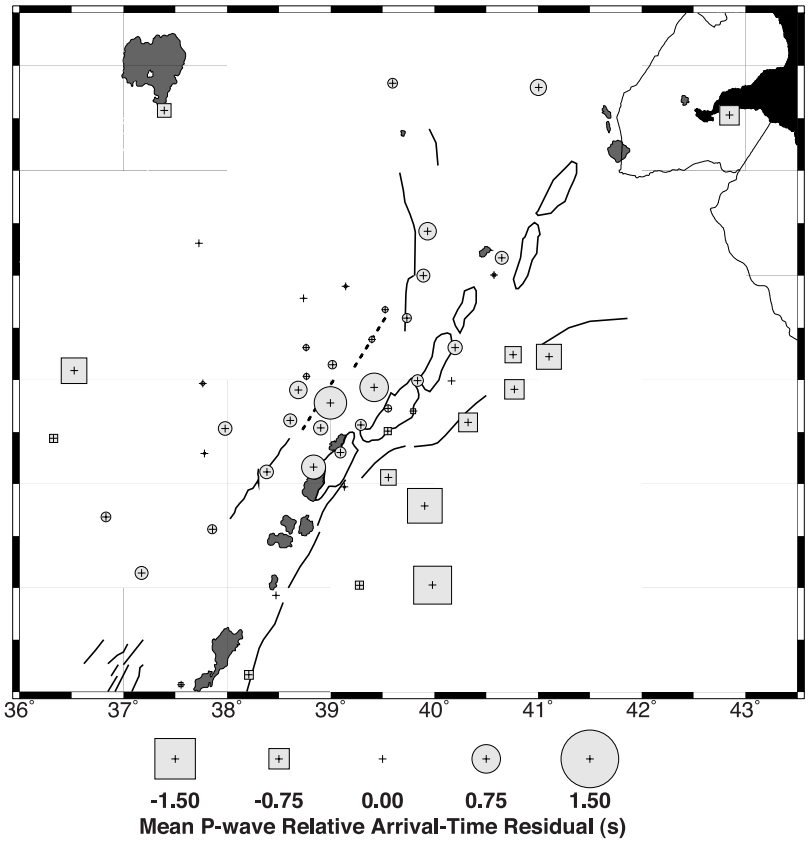
36° 37° 38° 39° 40° 41° 42° 43°
-1.50 -0.75 0.00 0.75 1.50
Mean P-wave Relative Arrival-Time Residual (s)

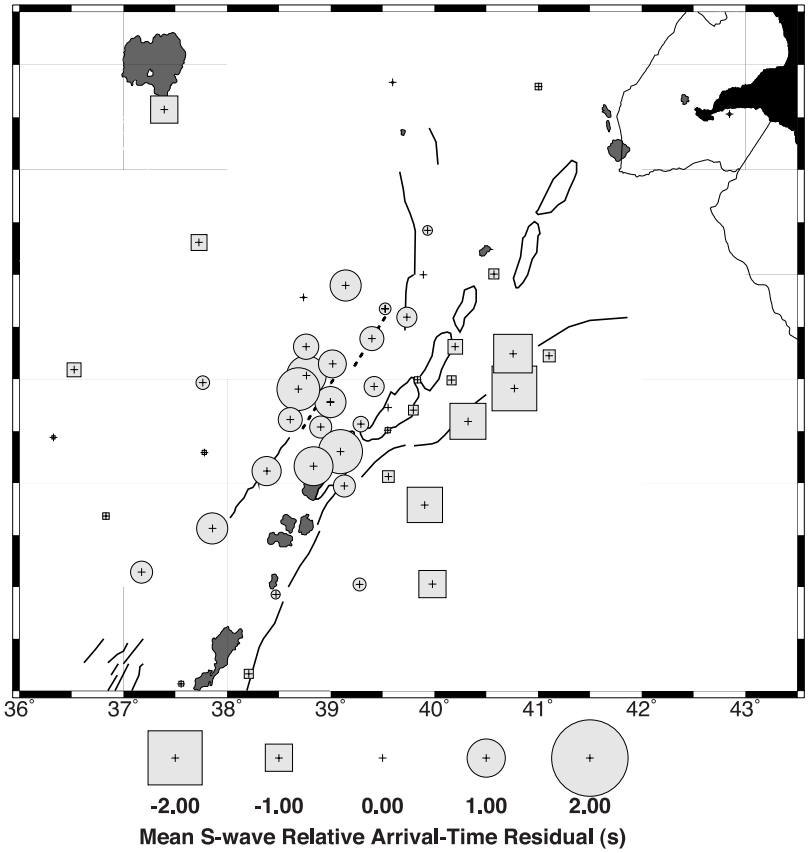
36° 37° 38° 39° 40° 41° 42° 43°
-2.00 -1.00 0.00 1.00 2.00
Mean S-wave Relative Arrival-Time Residual (s)

Figure 4

[24] Since our inverse problem is underdetermined (more unknowns than observations), even in the absence of errors we cannot expect to find a unique solution. We therefore choose to select a model that contains the least amount of structure [e.g., *Constable et al.*, 1987; *Allen et al.*, 2002; *Bastow et al.*, 2005]. The nonlinearity of the problem is addressed in the inversion procedure by performing 3-D ray tracing through successive linear inversion models. One iteration of 3-D ray tracing is performed for *P* waves in this study, with a ~10% loss of rays. We do not perform 3-D ray tracing for our *S* wave inversion because of problems converging a sufficient number of rays.

[25] By investigating the trade-off between the RMS residual reduction (the percent difference between the initial and final RMS misfit to the traveltime equations) and RMS model roughness we select a preferred model that fits the data well but does not account for more relative arrival time residual reduction than can be justified by our a priori estimation of data noise levels. All models in this study account for 94% (from 0.52 s to 0.03 s) of the RMS of the relative arrival time residuals for *P* waves and 91% (from 1.13 s to 0.10 s) for *S* waves. We are therefore treating our estimates of RMS timing uncertainty (0.02 s, and 0.05 s for *P* and *S* waves, respectively) as optimistic bounds when fitting the data. Station static terms computed during the inversion of the observed data are shown in Figures 7b and 9b. Subtracting the station terms from the delay times reduces the RMS of the relative arrival time residuals from 0.52 to 0.46 s for *P* waves and from 1.13 to 1.04 s for *S* waves; these corrected residuals reflect more accurately the proportion of the delay time anomalies that will be mapped into the region of the model where we make our interpretations.

3. Resolution

[26] Combining data from two major experiments increases the spatial coverage and station density of our study compared to earlier studies [e.g., *Bastow et al.*, 2005; *Benoit et al.*, 2006a, 2006b]. The increased number of station-earthquake pairs and network operation time also increases the expected resolving power of our combined data set. In an earlier study, *Bastow et al.* [2005] investigated the nonlinear resolving power of the EAGLE data set (3243 *P* wave and 1150 *S* wave traveltime observations) and found good lateral and vertical resolution in the region of the MER to ~300 km depth. *Bastow et al.* [2005] also showed via synthetic tests that structures ≥75 km beneath the EAGLE network were independent of crustal structure: station static corrections accounted successfully for the shallower structures. *Benoit et al.* [2006a] and *Benoit et al.* [2006b] showed that the data from the Ethiopia Broadband Seismic Experiment could resolve broad-scale (~200 km diameter) *P* and *S* wave velocity structures in the Ethiopian upper mantle at 150–500 km depth but not at lithospheric depths (<150 km) beneath the Ethiopian Plateau.

[27] We assess the resolving power of the inversion technique in this study by analyzing the ability of our ray geometry to retrieve a checkerboard model using raypaths through a 1-D Earth. In the checkerboard test we place positive and negative slowness-anomaly (V_P = ±6%) spheres described by Gaussian functions across their diameter in three layers at 100, 300, and 500 km depth (Figures 5a and 5b). The checkerboard approach allows us to assess the sensitivity of our model by highlighting areas of good ray coverage and the extent to which smearing of anomalies occurs.

[28] We invert for these synthetic velocity structures using identical model parameterization and inversion regularization as used during the inversion of the observed data. A Gaussian residual time error component with a standard deviation of 0.02 s is added to the theoretical *P* wave traveltimes (the standard deviation of noise estimated for our observed data).

[29] Lateral resolution and recovery of the amplitudes of the anomalies (~50%) (Figures 5d, 5e, and 5f) is excellent throughout the model, with recovery of the spheres best at ~300 km where we expect a network of our dimensions to have the highest density of crossing rays [e.g., *Ritsema et al.* 1998]. Vertical resolution is also good (Figure 5c) to depths approaching the transition zone (410–660 km). The quality and spatial extent of the resolution obtained in the present study is an improvement on that achieved by the earlier studies of *Bastow et al.* [2005, Figures 5 and 6], *Benoit et al.* [2006a, Figure 5], and *Benoit et al.* [2006b, Figure 3], particularly beneath the NW Plateau.

[30] In addition to the checkerboard test, we assess resolution by computing traveltimes through a synthetic rift model that simulates the kind of structure we see in our observed data inversions. This model (Figure 6) has rift flanks (peak velocity perturbation δV_P = +3%) and a tabular low-velocity body (δV_P = −5%) beneath the MER. The high- and low-velocity anomaly bodies are defined

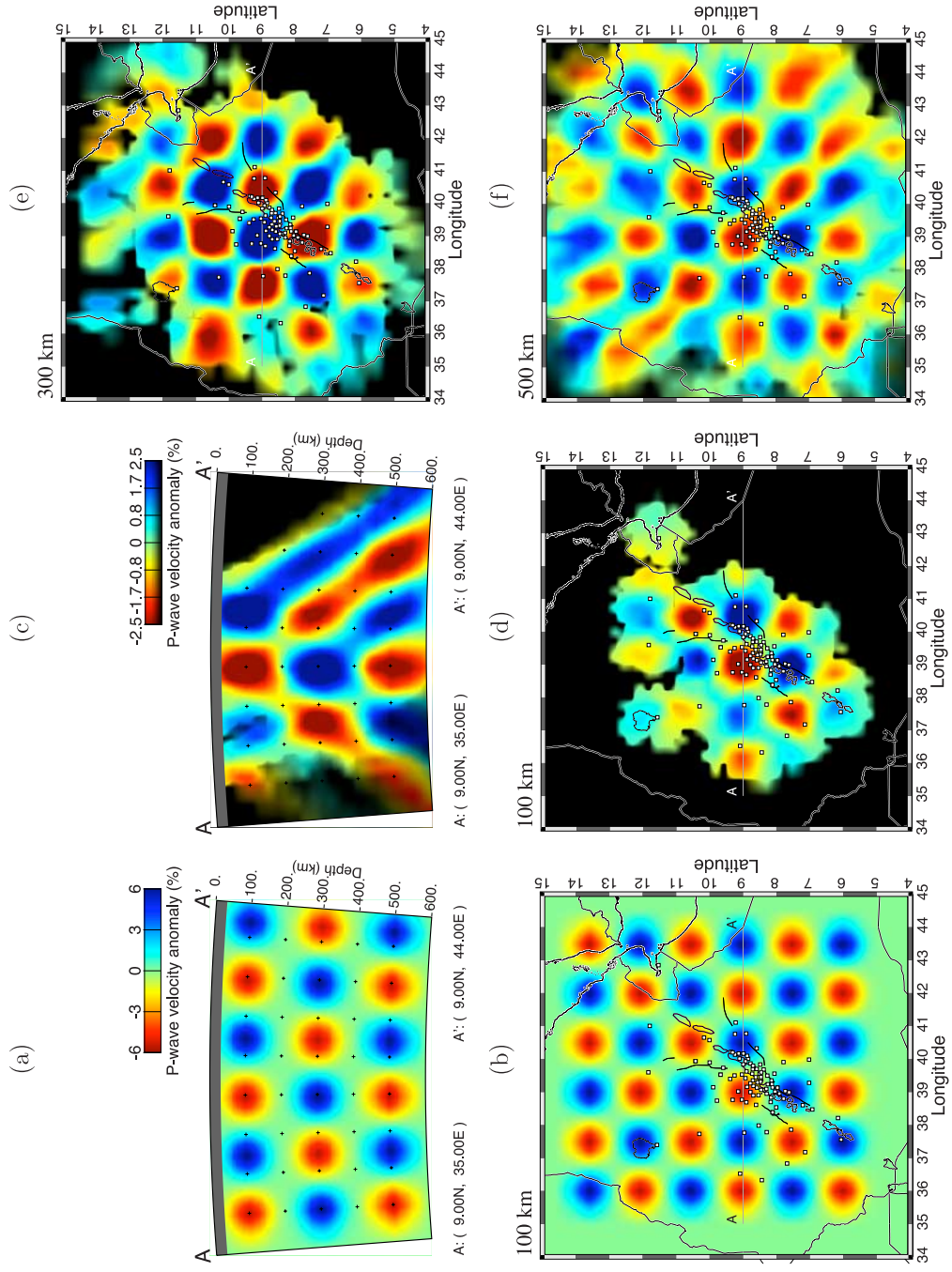

Figure 5. (a and b) Cross section and 100 km depth slice through the synthetic checkerboard model. Spheres of diameter 55 km (defined by Gaussian functions across their diameter) of $\delta V_P = \pm 6\%$ peak anomaly are distributed in layers of depth 100, 300, and 500 km in order to simulate small-scale velocity heterogeneity in the uppermost mantle beneath the study area. (c) Cross section through the retrieved checkerboard model. (d, e, and f) Depth slices through the retrieved checkerboard model at 100, 300, and 500 km depth. The grey bands at the top of the cross sections preclude the view of the uppermost unresolved part of the model where ray paths are almost all parallel and vertical. Black lines in the depth slices show locations of Quaternary magmatic centers and mid-Miocene border faults, respectively. Political boundaries and lakes are shown in black and white. Areas of low ray density (less than 10 rays per 25 km^3) are black.

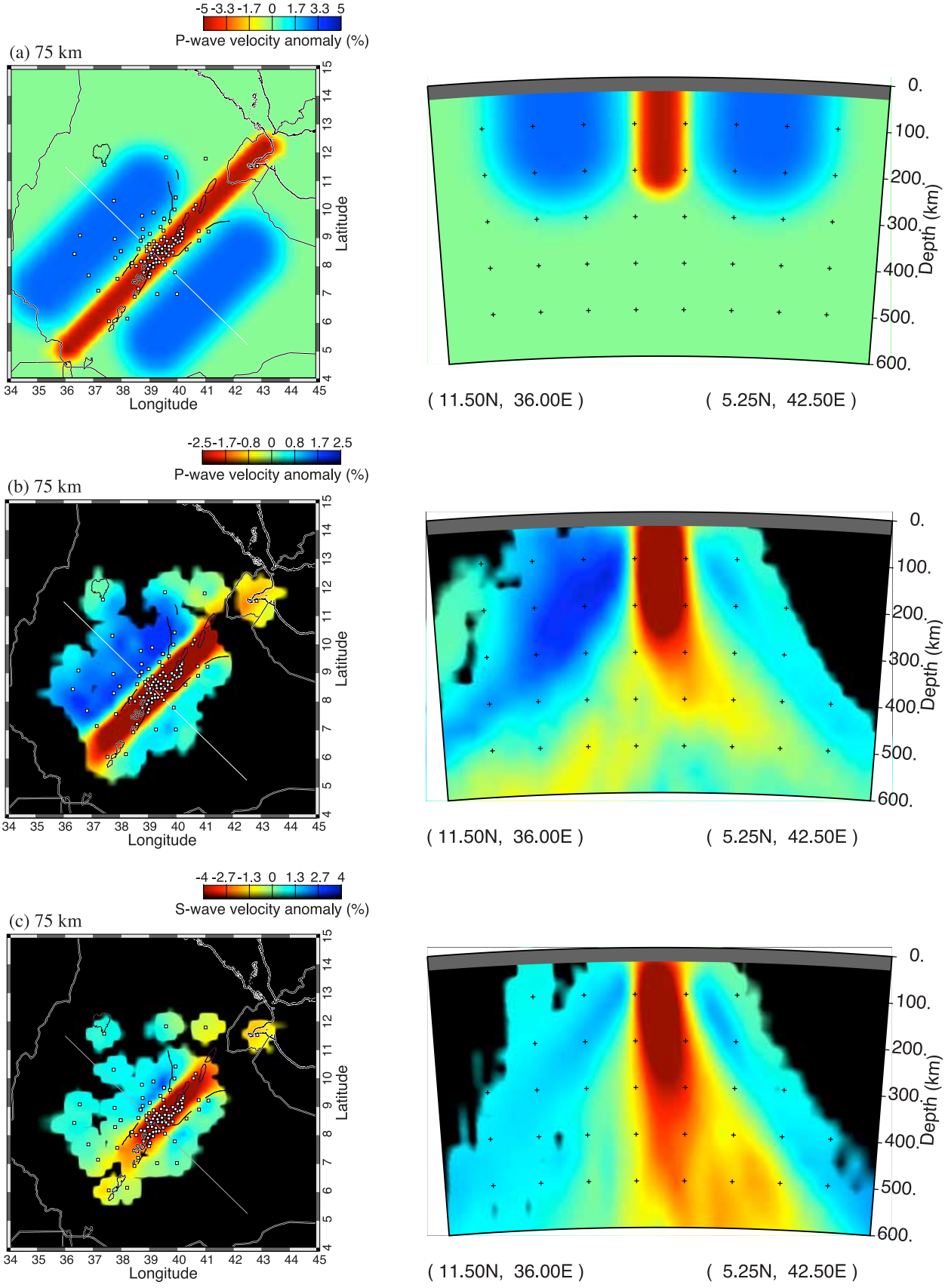
-5 -3.3 -1.7 0 1.7 3.3 5
P-wave velocity anomaly (%)
(a) 75 km
Latitude
Longitude
0.
100.
200.
300.
400.
500.
600.
Depth (km)
(11.50N, 36.00E)
(5.25N, 42.50E)
-2.5 -1.7 -0.8 0 0.8 1.7 2.5
P-wave velocity anomaly (%)
(b) 75 km
Latitude
Longitude
Depth (km)
(11.50N, 36.00E)
(5.25N, 42.50E)
-4 -2.7 -1.3 0 1.3 2.7 4
S-wave velocity anomaly (%)
(c) 75 km
Latitude
Longitude
Depth (km)
(11.50N, 36.00E)
(5.25N, 42.50E)

Figure 6

by Gaussian functions across their width and extend with peak anomaly from 0 to 225 km, falling to zero anomaly at ~275–300 km. Lateral resolution is excellent in the upper ~250 km with no noticeable offset or segmentation of the low-velocity tabular body beneath the MER (Figure 6b). Amplitude recovery is ≥50% beneath the MER and NW Plateau but drops to ~25% beneath the Somalian Plate. Vertical resolution is good beneath the MER and the NW Plateau within ~200 km of the rift; anomalies are smeared downward by ≤100 km.

[31] Figure 6 also shows the results of our *S* wave synthetic model, which has initial peak velocity anomaly amplitudes of $\delta t_S = -10\%$ and +6% for the rift and rift flanks, respectively. These results show that the rift model can be retrieved successfully using the smaller *S* wave data set, but the extent of the vertical smearing is greater than in the *P* wave case.

[32] Our improved resolution in this study compared to the earlier work by *Bastow et al.* [2005] and *Benoit et al.* [2006a, 2006b] will allow for more detailed analyses of rifting and hot spot tectonic processes in Ethiopia, especially in the shallow mantle (<150 km) beneath the NW Plateau.

4. Upper Mantle Seismic Structure

[33] Depth slices through the *P* wave velocity model at 75–350 km depth (Figure 7) reveal a broad (~500 km wide) low-velocity ($\delta V_P \approx -1.0\%$ relative to the background mean) zone that extends from the eastern flank of the MER westward beneath the uplifted NW Plateau. The northwest boundary of this LVR appears to exist near station BAHI (Figure 1). To the NW of BAHI, a region of high-velocity ($\delta V_P = 1.5\%$) structure is imaged throughout the upper 400 km of the model ~400 km from the MER. Similarly, low velocities give way to high velocities on the Somalian Plate ~150 km from the MER. To first order, the broad LVR underlies regions of maximum uplift in Ethiopia, principally the NW Plateau to the west of the MER, and the Bale Mountains on the Somalian Plate (Figure 1). In cross section, the LVR exists throughout the upper 400 km of the mantle (Figure 8), consistent with the results of *Benoit et al.* [2006a]. At 75–150 km depth, lowest velocities are seen in the latitude range 7–10°N (Figures 7a and 7b), consistent with our observations of latest mean relative arrival time residuals (Figure 3).

[34] Within the broad LVR we image regions of smaller-scale seismic heterogeneity. The rift shoulders are characterized by relatively faster (up to $\delta V_P = 1.5\%$) velocity structure within ~50 km of the rift. The lateral extent of these high-velocity zones away from the MER was previously unknown due to poor resolution beneath the plateau [*Bastow et al.*, 2005], but we now image them as discrete ≥50 km-wide zones near the rift shoulders at 10°N, 39°E, at 9.5°N, 41°E, and at 8°N, 40.5°E, for example (Figure 7a). Cross sections through these high-velocity zones indicate that they extend to ~100 km depth (Figure 8, B-B′).

[35] Along the length of the MER at 75 km depth, low-velocity anomalies ($\delta V_P = -1.5\%$) are consistently offset from the center of the rift toward the higher flanks (Figure 7a), consistent with the earlier study of *Bastow et al.* [2005]. Below ~100 km depth the low-velocity anomalies become more central about its axis. North of ~10°N, the MER LVR at 75 km depth (Figure 7a) shifts eastward and follows the trend of the younger MER that may overprint the Late Oligocene Red Sea and Gulf of Aden rift structures [e.g., *Wolfenden et al.*, 2004].

[36] A limb of low-velocity structure at 75 km depth (Figure 7a) extends from the NNE-trending MER to the west of 9°N, 39°E and ≥100 km in a westerly direction from the Boset volcanic zone in the center of the rift (Figure 1). This limb corresponds to an area of lower relief bounded to the north by the E-W striking Yerer Tullu Wellel Volcanic Lineament (YTVL) [*Mohr*, 1967] and the northern portion of the SDFZ that is characterized by numerous Quaternary eruptive centers [e.g., *WoldeGabriel et al.*, 1990; *Abebe et al.*, 1998; *Rooney et al.*, 2005]. Another isolated anomaly underlies the southern margin of the Aden rift, near station MIEE (Figures 1 and 7a). Gara Gumbi, a large Late Miocene trachytic volcano, lies above the eastern side of this velocity anomaly [e.g.,

Figure 6. (a) Depth slice (shown on the left) through input *P* wave synthetic rift model at 75 km depth. The white line on this figure indicates the location of the cross section (shown on the right). (b) Depth slice (shown on the left) and cross section (shown on the right) through the recovered *P* wave synthetic rift model. (c) Depth slice (shown on the left) and cross section (shown on the right) through the recovered *S* wave synthetic rift model.

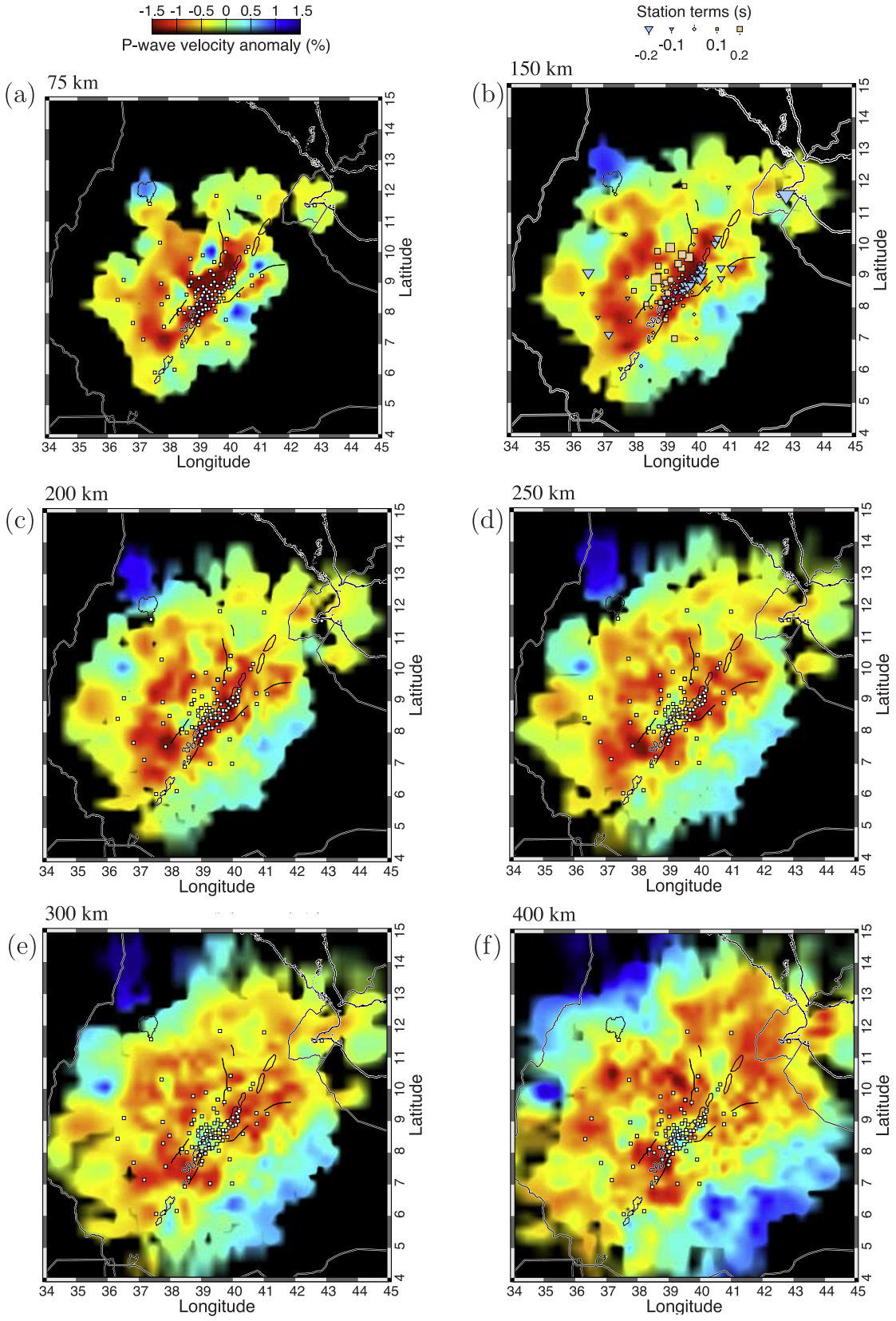

Figure 7. Depth slices through the *P* wave velocity model at 75, 150, 200, 250, 300, and 400 km depth. (a, c–f) The locations of the stations contributing to the tomographic inversions are shown in the white squares. (b) Square and triangular symbols show the magnitude and sign of the station static terms.

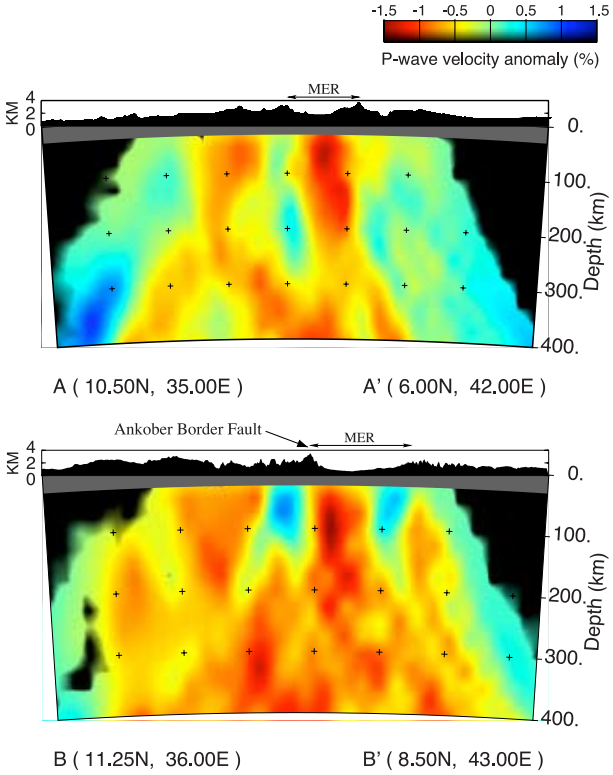

Figure 8. (top) A-A′ shows the vertical cross sections through the *P* wave velocity model in the continental rifting part of the study area. (bottom) B-B′ shows the cross section through the transitional rifting region toward Afar. Orientations of the cross sections are shown as grey lines in Figure 6a.

Chernet et al., 1998]. Further correlations between preexisting lithospheric structural trends and LVR are seen beneath the NW Plateau south of ~7.5° where rift zones span a ~500 km wide area across which the MER has migrated eastward to its present day location [e.g., *Ebinger et al.*, 2000].

[37] Cross sections through the *P* wave velocity model (Figure 8, A-A′) reveal a narrow (~75 km-wide) tabular LVR beneath the southern, less extended part of the MER extending to ≥300 km depth. Further north, toward the Afar depression, a narrow LVR offset toward the Ankober Border Fault (Figure 1) only extends to ~150 km depth before it broadens laterally with depth (Figure 8, B-B′). A limb of low-velocity material also exists beneath the eastern rift flank beneath stations MIEE, BEDE, HIRE, and MECE (Figure 1). Middle upper-mantle velocity structure (200–400 km depth) is a complex network of low velocities throughout the study area. We acknowledge, however, that some of the apparent heterogeneity at these depths will be the result of imperfect amplitude recovery during the inversion procedure, but our good resolution (Figures 5 and 6) means we have strong evidence to suggest that there is some linkage between shallow (≤300 km depth) and deeper LVRs.

[38] Our independently inverted *S* wave data (Figure 9) confirm the first-order observations from the *P* wave study but the finer-scale structures are less well defined in the *S* wave model. We attribute this to the lower resolving power of the *S* wave data set that has fewer rays than the *P* wave study; seismic wavelengths are also longer in the *S* wave study. *S* wave data are also noisier since they are picked on horizontal component seismograms. It is notable that the lowest *S* wave velocities are generally closer to the rift valley than in the *P* wave case. Station static terms computed within the inversions are shown in Figures 7b and 9b.

5. Discussion

[39] In summary, the main new observations from our seismic models are as follows: (1) there is a broad (~500 km wide) LVR under Ethiopia that extends downward from lithospheric depths to the transition zone, (2) the MER has formed toward the eastern flank of this LVR, (3) velocities are lower beneath central Ethiopia compared to Afar, and (4) within the broad LVR, there is significant lateral heterogeneity at sublithospheric depths. In this section, we use these observations to address outstanding questions about the origin, nature, and evolution of the Ethiopia/Afar hot spot. We also pose the question of what role the lithosphere has played in rift development.

5.1. Partial Melt in the Upper Mantle?

[40] Seismic heterogeneities within the Earth can arise, for example, due to changes in temperature, composition, and partial melt [e.g., *Karato*, 1993; *Goes et al.*, 2000]. *Bastow et al.* [2005] used a range of temperature derivatives (δV_P = 0.5–2% per 100°C; δV_S = 0.7–4.5% per 100°C) to account for anelastic and anharmonic effects on seismic velocities [e.g., *Karato*, 1993; *Goes et al.*, 2000] to estimate a hypothetical 122–800°C temperature variation between the MER and adjacent rift shoulders at ~150 km depth. Note that these calculations assume the seismic heterogeneities are entirely of a thermal origin and are intended only to investigate end members of the temperature hypothesis. A high-temperature hypothesis for Ethiopia is favored if the upper mantle material

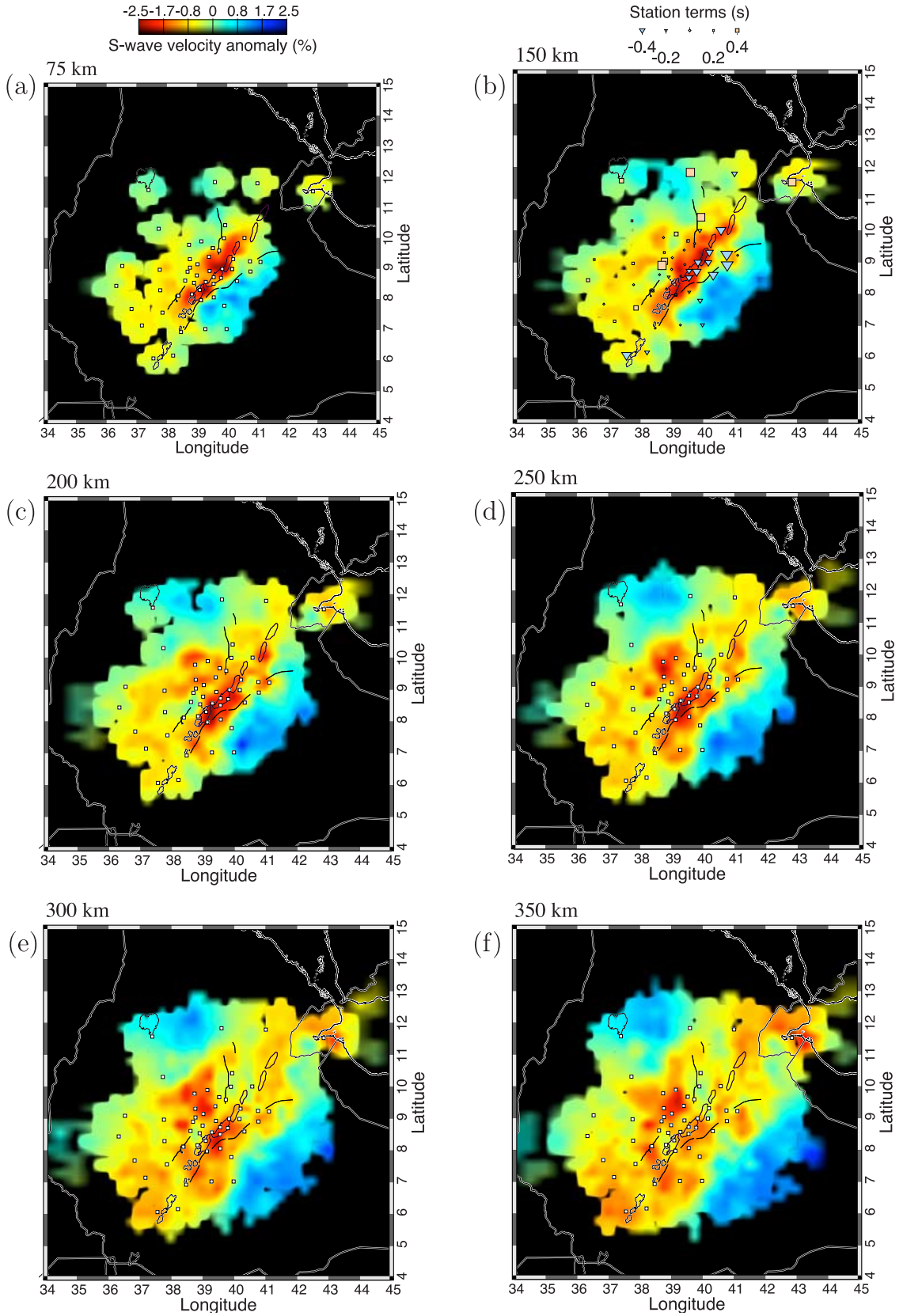

Figure 9. Depth slices through the *S* wave velocity model at 75, 150, 200, 250, 300, and 350 km depth. (a, c–f) The locations of the stations contributing to the tomographic inversions are shown in the white squares. (b) Square and triangular symbols show the magnitude and sign of the station static terms.

we image has lower mantle origins since *Ni et al.* [2002] and *Simmons et al.* [2007] infer a thermally induced positive buoyancy contribution to the African Superplume in the lower mantle. However, the upper temperature estimates above are implausible on the basis of other global hot spots (e.g., Iceland; 140–200°C) [*Allen et al.*, 2002, and references therein] so factors in addition to or alternative to high temperatures must be considered.

[41] Our observations of absolute delay times in Ethiopia indicate a ~6% decrease in upper-mantle δV_P is necessary for comparison with standard Earth models. Our *P* wave images therefore provide a strong case for the presence of partial melt beneath the MER and adjacent NW Plateau to depths in excess of those inferred for the source of Quaternary lavas in the MER (50–90 km) [*Rooney et al.*, 2005]. In the *S* wave model, lowest velocity zones are particularly confined to the region of the MER (Figure 9a), so it is here that melt volumes are probably largest in Ethiopia. *Bastow et al.* [2005] analyzed *P* and *S* wave traveltimes for EAGLE network stations to show that some degree of partial melt was necessary in the Ethiopian upper mantle in order to explain the seismic observations. Melting even in a dry fertile mantle peridotite is highly pressure dependent and decompressional melting in response to lithospheric stretching [e.g., *White and McKenzie*, 1989] likely contributes to the observed low seismic velocities beneath the extending MER and Afar.

[42] In addition to thermally derived partial melt, composition can affect seismic velocities [e.g., *Deschamps et al.*, 2002]. Depletion of the subcontinental lithospheric mantle of lower melting point components may cancel thermal effects on density [e.g., *Jordan*, 1988] and by inference velocity. The presence of water in the mantle can significantly reduce seismic velocities which, in turn, can promote melting at constant temperatures [e.g., *Nichols et al.*, 2002]. Compositional effects are generally considered secondary to temperature [e.g., *Goes et al.*, 2000; *Cammarano et al.*, 2003; *Faul and Jackson*, 2005] in the upper mantle, however.

[43] Whatever the cause, a partial melt hypothesis for Ethiopia seems essential and is consistent with geochemical and geophysical results that point toward a MER model characterized by ongoing intrusion of dikes of magma rising from the base of the lithosphere [e.g., *Rooney et al.*, 2005; *Kendall et al.*, 2005, 2006] and into the crust, where mafic intrusions achieve much of the extension [*Ebinger and Casey*, 2001; *Keranen et al.*, 2004; *Mackenzie et al.*, 2005; *Rooney et al.*, 2005; *Daly et al.*, 2008]. Magnetotelluric studies [*Whaler and Hautot*, 2006] indicate the lower crust beneath the NW Plateau is more conductive than the Somalian Plate and that melt zones exist in the crust beneath the MER in the upper ~25 km.

5.2. Plume Structure

[44] In this section, we consider whether our *P* and *S* wave relative arrival time residuals and velocity models are consistent with the plume models proposed to explain Ethiopia's uplift and hot spot tectonic history. Large-amplitude velocity anomalies in the upper mantle preclude the possibility that the MER is a passive rift [*Bastow et al.*, 2005] but our results provide no evidence for a narrow (~100–200 km diameter) plume tail beneath Ethiopia, as would be expected if a starting thermal plume existed today. It has recently been proposed that the broad African Superplume is one of Earth's oldest mantle features [e.g., *Ni and Helmberger*, 2003], though our present-day snapshot of the mantle does not preclude the possibility that one or more starting plumes may have existed beneath Ethiopia during Eocene-Oligocene times [*Schilling et al.*, 1992; *Burke*, 1996; *Ebinger and Sleep*, 1998; *George et al.*, 1998; *Furman et al.*, 2006].

[45] Many seismic studies that probe deeper portions of the African mantle reveal a broad (~500 km wide) low-velocity ($\delta V_S \approx 3\%$) zone that extends from the core-mantle boundary beneath southern Africa [e.g., *Lithgow-Bertelloni and Silver*, 1998; *Gurnis et al.*, 2000; *Ni et al.*, 2002; *Ritsema and Allen*, 2003; *Simmons et al.*, 2007; *Li et al.*, 2008] and into the upper mantle beneath Ethiopia [*Benoit et al.*, 2006a, 2006b]. Regional-scale surface wave studies also provide support for a broad LVR of upwelling in the Ethiopian mantle [e.g., *Debayle et al.*, 2001]. The most significant peak-to-peak variations in *P* wave relative arrival time residuals in our study (Figure 3) indicate that the largest lateral velocity variations in Ethiopia lie somewhere near or beyond the edges of our seismic network, west of station BAHI (11.57°N, 37.39°E: Figure 1). This observation is consistent with the existence of the broad (~500 km wide) LVR beneath Ethiopia that we image in Figures 7, 8, and 9.

[46] The center of the mantle LVR at depths ≥150 km is located beneath the NW Plateau, not the MER or Afar (Figures 4, 7, and 9), in contrast

to many global scale tomographic studies [e.g., *Ritsema and Allen*, 2003; *Montelli et al.*, 2004, 2006]; this discrepancy is likely the result of our significantly better data coverage in Ethiopia. The observations are corroborated by mean and maximum relative arrival time residuals (Figures 3 and 4), which do not suffer the same resolution problems as the tomographic images. Note also that shear wave splitting studies indicate a peak in delay time at this latitude; these measurements are interpreted in terms of melt inclusion within the lithosphere [*Kendall et al.*, 2005, 2006]. The upper-mantle velocities observed in the MER could indicate that the most intense zone of present-day upwelling lies further south than previously thought, though alternative hypotheses exist. Enhanced decompressional melting might be expected beneath the MER at 8.5–10.5°N since it is the most recently formed part of the EAR in Ethiopia. On the basis of recent geochemical studies, this part of the MER may be the junction between two separate rift systems: the southward propagating Red Sea rift and the northward propagating EAR [e.g., *Rooney et al.*, 2007]. Kinematic rifting models indicate that rapid lithospheric thinning can result in decompressional melting of the underlying mantle [e.g., *Bown and White*, 1995]. Rifting over longer periods, however, greatly reduces melt volumes as heat is lost through conduction. Such ideas, coupled with greater depletion of the subcontinental lithospheric mantle beneath Afar, could explain our seismic observations, with larger melt volumes producing the lower velocities in the MER.

[47] Isotopic studies of modern magmatism in Afar, the Red Sea, Gulf of Aden, and MER [e.g., *Schilling et al.*, 1992; *Furman et al.*, 2006] and of the 30 Ma Ethiopian/Yemen flood basalt province [e.g., *Baker et al.*, 1996; *Pik et al.*, 1999] all require the input of a plume component in order to explain the observed geochemical variations. *Furman et al.* [2006] indicate that this isotopic plume signature has remained essentially constant over the last 30 Ma, suggesting the Afar plume is a long-lived feature. Magmatism in southern Ethiopia/Kenya has also been attributed to mantle plume activity [e.g., *George et al.*, 1998; *Rogers*, 2006; *Furman et al.*, 2006]; however, the relationship of this plume to the Afar plume remains unclear. Heterogeneities in the LVR we image at 200–400 km depth (Figures 7, 8, and 9) could be indicative of smaller upwellings from the underlying African Superplume, consistent with numerical models [e.g., *Farnetani and Samuel*, 2005] and geochemical evidence that supports a complex upwelling and a modified single plume theory [*Furman et al.*, 2006].

5.3. Rift Initiation and Development

[48] From our velocity models it appears that the MER formed toward the eastern edge of the mantle LVR, not directly above it [e.g., *Rogers*, 2006]. We investigate whether this offset is due to lithospheric structures influencing MER location and development. To what extent have seismic heterogeneities at lithospheric depths (Figures 7a and 9a) developed in response to preexisting lithospheric structural trends as opposed to Miocene-Recent extensional tectonism?

5.3.1. Rift Initiation

[49] Some features in our velocity models correlate with lithospheric features that predate Miocene-Recent rifting in Ethiopia (e.g., the E-W trending YTVL; Figures 1 and 7a). The $\geq$50 km-wide high-velocity zones that characterize the rift shoulders at $\sim$75 km depth (Figures 7, 8, and 9) could be depleted lithospheric mantle zones. The high-velocity zone around 9.5°N, 41°E, for example, is overlain by several Miocene-Pliocene silicic centers: Asebot, Afdem, Bora At, Gara Adi, and Gara Gumbi [e.g., *Chernet et al.*, 1998, Figure 1]. In most other areas, however, volcanic centers such as Guna, Choke, and Guguftu (Figure 1) are underlain by low-velocity material (Figures 7a and 9a). The depth extent of the high-velocity zones (Figure 8, B-B′) is $\sim$100 km, which allowing for a modest amount of vertical smearing (Figure 5c), matches 70–80 km depth estimates for the base of the NW Plateau lithosphere [*Dugda et al.*, 2007]. High-velocity zones may therefore be zones of strong/old/cold lithosphere whose greater residual strength compared to the surrounding lithosphere have played an important role in defining the present day location of the MER. Although we do not preclude the chemical depletion hypothesis entirely, our observations could, therefore, be interpreted as supportive of rifting models in which lithospheric structural inheritances influence the early stages of rifting [e.g., *Vauchez et al.*, 1997; *Keranen and Klemperer*, 2007].

[50] Other geophysical studies also support the concept of rift initiation along lithospheric structural inheritances. Wide-angle seismic studies [*Mackenzie et al.*, 2005; *Maguire et al.*, 2006], receiver function data [*Dugda et al.*, 2005; *Stuart et al.*, 2006], and modeling of gravity anomalies

[*Cornwell et al.*, 2006] all infer asymmetric crustal structure across the MER, with crust ~15 km thicker to the west than the east. The lower crust (≥25 km) beneath the Somalian Plate is significantly more resistive than beneath the NW Plateau on the basis of magnetotelluric studies [*Whaler and Hautot*, 2006]. At lithospheric depths, *Dugda et al.* [2007] use joint inversion of receiver function and surface wave data to infer the existence of a "low-velocity lid" beneath the NW Plateau, consistent with our seismic images at 75 km depth (Figures 7a, 8, and 9a). Late Paleozoic-Mesozoic marine sediments are exposed on the Somalian Plate, but basement structural trends on the NW Plateau are mostly capped by thick sequences of flood basalts and rhyolites [e.g., *Tadesse et al.*, 2003]. Hence, correlations of velocity heterogeneities with lithospheric structures is not straightforward, though intraplateau uplift, rifting and subsidence in the Tana basin show that the NW Plateau is not a simple, undeformed structural block.

[51] Much of the crustal-scale asymmetry in plateau structure has been attributed to underplating emplaced during the eruption of Oligocene flood basalts with subsequent modification during recent rifting [e.g., *Maguire et al.*, 2006]. Underplating is a feature of all continental volcanic margins [e.g., *Kelemen and Holbrook*, 1995] but ~7 km thickness 7.0–7.3 km s^{-1} velocity lower crustal layers are commonly observed in Proterozoic crust worldwide [e.g., *Christensen and Mooney*, 1995] and may indicate a longer-standing asymmetry in plateau structure in Ethiopia than implied by the underplate hypothesis alone. In the following section we examine correlations between velocity anomalies and lithospheric structures to show that heterogeneities in lithospheric structure continue to play an important role in the structural development of the MER.

5.3.2. Rift Development

[52] Large offset border faults accommodated early extension in the MER [*Hayward and Ebinger*, 1996] before localized magma injection within the rift became the Quaternary locus of extension [e.g., *Ebinger and Casey*, 2001; *Keranen et al.*, 2004]. *Buck* [2006] emphasizes the importance of magma intrusion in the early stages of rifting as a means of explaining the straightness of rifts such as the Red Sea and MER but also acknowledges that terminations of straight rift segments are expected when dykes cannot penetrate thick lithosphere.

[53] *Bastow et al.* [2005] cited the lateral offset of LVRs away from the axial center of the rift (The WFB, Figure 1) toward the uplifted rift flanks as evidence that mid-Miocene border faults remain important today in determining the location of mantle upwellings beneath the rift. Our results confirm these observations in the latitude range 7.5°–10.5°N (Figures 7a, 8, and 9a), but our greater spatial coverage now enables us to develop these ideas further and to place the results of the earlier study in context with the surrounding Plateau structure.

[54] South of ~7.5°N, low velocities extend westward from the MER across a ~500 km wide zone of rifting that formed since Miocene times as the MER migrated eastward toward its present-day location [e.g., *Ebinger et al.*, 2000, Figures 7a and 8a]. This LVR is also noted in joint receiver function and surface wave analyses [e.g., *Dugda et al.*, 2007].

[55] Many rifting models emphasize magmatic intrusion of mafic material into the crust as evidence that the MER has evolved to an almost exclusively magmatic extensional system [e.g., *Ebinger and Casey*, 2001; *Buck*, 2006]. Our results are consistent with these models, but the greater depth extent of our study enables us to highlight the fact that the mid-Miocene border faults overlie regions of low velocity inferred to be melt migration pathways, despite them no longer being the principal locus of extension.

5.3.3. Transition to Seafloor Spreading

[56] Several studies have cited crustal-scale evidence in the MER to suggest that Ethiopia captures the transition from continental rifting to oceanic spreading [e.g., *Ebinger and Casey*, 2001; *Keranen et al.*, 2004; *Rooney et al.*, 2005]. The upper mantle beneath the MER at <75 km depth (Figures 7 and 9) has not yet organized itself into a series of punctuated magmatic upwellings as is expected beneath a fully developed seafloor spreading center [e.g., *Kuo and Forsyth*, 1988; *Phipps-Morgan and Chen*, 1993; *Gregg et al.*, 2007]. South of ~10°N, the locations of LVRs at lithospheric depths remain strongly controlled by Miocene-to-recent (rifting) related lithospheric structural trends (border faults) and do not mirror Quaternary magmatic segmentation of the crust (Figures 7a and 9a). Though poorly resolved we speculate that northern Afar (>10°N) might be the stage in the transitional rifting process where the mantle organizes itself

into punctuated upwellings beneath a protoseafloor spreading center.

6. Conclusions

[57] By successfully combining broadband teleseismic traveltime data from two recent major temporary deployments in East Africa, we present the most detailed tomographic images to date of *P* and *S* wave seismic velocity structure beneath a 650 × 750 km area in Ethiopia to a depth of ~400 km.

[58] *P* and *S* wave traveltime analyses and new tomographic images indicate that a broad (~500 km wide) SW-NE trending upper mantle low-velocity zone underlies the MER and much of the adjacent flood basalt capped NW Plateau. This broad LVR is interpreted as the upper mantle continuation of the African Superplume. The MER has not formed directly above the mantle LVR, but toward its eastern edge.

[59] Within the broad low-velocity anomaly, the lowest-velocity zones, interpreted as zones of partial melt, are located at ~9°N in the MER, not beneath Afar. This result contrasts with many global tomographic studies but it is unclear whether the intense LVR has resulted from focused mantle upwelling and/or enhanced decompressional melting at this latitude, where the MER is a younger lithospheric feature than Afar to the north and the East African Rift to the south. Models for rifting in which a S-N increase in melt volume accompanies the transition from continental rifting to oceanic spreading may not be appropriate. The MER likely formed in a discontinuous manner, with lithospheric structure playing an important role in its evolution.

[60] Whatever the model for rifting in Ethiopia, our study provides clear evidence for an abundant source of partially molten upper mantle material that is subsequently incorporated into the crust and lithospheric mantle where GPS data indicate it accommodates ~80% of present day strain in the MER [e.g., *Bilham et al.*, 1999]. In this respect, our results are consistent with the magma assisted rifting hypothesis of *Buck* [2004, 2006] but future models for MER evolution should additionally incorporate the effects of Ethiopia's heterogeneous lithospheric structure.

Acknowledgments

[61] We thank John VanDecar for providing us with the inversion code used in this study. Tanya Furman reviewed early drafts and John Tarduno, Hans Thybo, Richard England, and Ullrich Achauer provided insightful reviews that improved the manuscript. Thomas Owens and J-Michael Kendall funded IB during the period 2005-8. This work has been partly supported by National Science Foundation grants EAR993093 and EAR0530062 and NERC grant NER/A/S/2000/01003. Laike Asfaw, Atalay Ayele, and their colleagues at Addis Ababa University are thanked for their support throughout the course of our experiments in Ethiopia.

References

Abebe, T., F. Mazzarini, F. Innocenti, and P. Manetti (1998), The Yerer–Tullu Wellel volcanotectonic lineament: A transtensional structure in central Ethiopia and the associated magmatic activity, *J. Afr. Earth Sci.*, *26*(1), 135–150.

Allen, R., et al. (2002), Imaging the mantle beneath Iceland using integrated seismological techniques, *J. Geophys. Res.*, *107*(B12), 2325, doi:10.1029/2001JB000595.

Baker, J., L. Snee, and M. Menzies (1996), A brief Oligocene period of flood volcanism in Yemen, *Earth Planet. Sci. Lett.*, *138*, 39–55.

Bastow, I. (2005), Upper-mantle seismic structure in a region of incipient continental break-up: Northern Ethiopian rift, Ph.D. thesis, Univ. of Leeds, Leeds, U.K.

Bastow, I., G. Stuart, J.-M. Kendall, and C. Ebinger (2005), Upper-mantle seismic structure in a region of incipient continental breakup: northern Ethiopian rift, *Geophys. J. Int.*, *162*(2), 479–493, doi:10.1111/j.1365-246X.2005.02666.x.

Benoit, M., A. Nyblade, J. VanDecar, and H. Gurrola (2003), Upper mantle P wave velocity structure and transition zone thickness beneath the Arabian Shield, *Geophys. Res. Lett.*, *30*(10), 1531, doi:10.1029/2002GL016436.

Benoit, M., A. Nyblade, T. Owens, and G. Stuart (2006a), Mantle transition zone structure and upper mantle S velocity variations beneath Ethiopia: Evidence for a broad, deep-seated thermal anomaly, *Geochem. Geophys. Geosyst.*, *7*, Q11013, doi:10.1029/2006GC001398.

Benoit, M., A. Nyblade, and J. VanDecar (2006b), Upper mantle P wavespeed variations beneath Ethiopia and the origin of the Afar hotspot, *Geology*, *34*(5), 329–332.

Berhe, S. (1990), Ophiolites in northeast and East Africa: Implications for Proterozoic crustal growth, *J. Geol. Soc. London*, *147*, 41–57.

Bilham, R., R. Bendick, K. Larson, P. Mohr, J. Braun, S. Tesfaye, and L. Asfaw (1999), Secular and tidal strain across the Main Ethiopian Rift, *Geophys. Res. Lett.*, *26*, 2789–2792.

Bown, J., and R. White (1995), Effect of finite extension rate on melt generation at rifted continental margins, *J. Geophys. Res.*, *100*(B9), 18,011–18,029.

Brown, G. (1970), Eastern margin of Red Sea and coastal structures in Saudi Arabia, *Phil. Trans. R. Soc. London, Ser. A*, *267*, 75–87.

Buck, W. (2004), Consequences of asthenospheric variability on continental rifting, in *Rheology and Deformation of the Lithosphere at Continental Margins*, edited by G. Karner et al., pp. 1–30, Columbia Univ. Press, New York.

Buck, W. (2006), The role of magma in the development of the Afro-Arabian Rift System, in *The Structure and Evolution of the East African Rift System in the Afar Volcanic Province*, edited by G. Yirgu, C. J. Ebinger, and P. K. H. Maguire, *Geol. Soc. London Spec. Publ.*, *259*, 43–54.

Burke, K. (1996), The African plate, *S. Afr. J. Geol.*, *99*, 339–409.

Cammarano, F., S. Goes, P. Vacher, and D. Giardini (2003), Inferring upper-mantle temperatures from seismic velocities, *Phys. Earth Planet. Inter.*, *138*, 197–222.

Chernet, T., W. Hart, J. Aronson, and R. Walter (1998), New age constraints on the timing of volcanism and tectonism in the northern Main Ethiopian Rift—Southern Afar transition zone (Ethiopia), *J. Volcanol. Geotherm. Res.*, *80*, 267–280.

Christensen, N., and W. Mooney (1995), Seismic velocity structure and composition of the continental crust, *J. Geophys. Res.*, *100*(B7), 9761–9788.

Constable, S., R. Parker, and C. Constable (1987), Occam's inversion: A practical algorithm for generating smooth models from electromagnetic sounding data, *Geophysics*, *52*, 289–300.

Cornwell, D., G. Mackenzie, P. Maguire, R. England, L. Asfaw, and B. Oluma (2006), Northern Main Ethiopian Rift crustal structure from new high-precision gravity data, in *The Structure and Evolution of the East African Rift System in the Afar Volcanic Province*, edited by G. Yirgu, C. J. Ebinger, and P. K. H. Maguire, *Geol. Soc. London Spec. Publ.*, *256*, 309–323.

Corti, G. (2008), Control of rift obliquity on the evolution and segmentation of the main Ethiopian rift, *Nat. Geosci.*, *1*(4), 258–262, doi:10.1038/ngeo160.

Courtillot, V., C. Jaupart, I. Manighetti, P. Tapponnier, and J. Besse (1999), On causal links between flood basalts and continental breakup, *Earth Planet. Sci. Lett.*, *166*, 177–195.

Daly, E., D. Keir, C. Ebinger, G. Stuart, I. Bastow, and A. Ayele (2008), Crustal tomographic imaging of a transitional continental rift: the Ethiopian Rift, *Geophys. J. Int.*, *172*(3), 1033–1048, doi:10.1111/j.1365-246X.2007.03682.x.

Debayle, E., J. Lévêque, and M. Cara (2001), Seismic evidence for a deeply rooted low-velocity anomaly in the upper mantle beneath the northeastern Afro/Arabian continent, *Earth Planet. Sci. Lett.*, *193*, 423–436.

Deschamps, F., J. Trampert, and R. Snieder (2002), Anomalies of temperature and iron in the uppermost mantle inferred from gravity data and tomographic models, *Phys. Earth Planet. Inter.*, *129*, 245.

Dugda, M., A. Nyblade, J. Julià, C. Langston, C. Ammon, and S. Simiyu (2005), Crustal structure in Ethiopia and Kenya from receiver function analysis, *J. Geophys. Res.*, *110*, B01303, doi:10.1029/2004JB003065.

Dugda, M., A. Nyblade, and J. Julià (2007), Thin lithosphere beneath the Ethiopian plateau revealed by a joint inversion of Rayleigh wave group velocities and receiver functions, *J. Geophys. Res.*, *112*, B08305, doi:10.1029/2006JB004918.

Ebinger, C., and M. Casey (2001), Continental breakup in magmatic provinces: An Ethiopian example, *Geology*, *29*, 527–530.

Ebinger, C., and N. Sleep (1998), Cenozoic magmatism throughout East Africa resulting from impact of a single plume, *Nature*, *395*, 788–791.

Ebinger, C., T. Yemane, G. WoldeGabriel, J. Aronson, and R. Walter (1993), Eocene-Recent volcanism and faulting in the southern Main Ethiopian rift, *J. Geol. Soc. London*, *150*, 99–108.

Ebinger, C., T. Yemane, D. Harding, S. Tesfaye, S. Kelley, and D. Rex (2000), Rift deflection, migration, and propagation: Linkage of the Ethiopian and Eastern rifts, Africa, *Bull. Geol. Soc. Am.*, *112*(2), 163–176.

Farnetani, C., and H. Samuel (2005), Beyond the thermal plume paradigm, *Geophys. Res. Lett.*, *32*, L07311, doi:10.1029/2005GL022360.

Faul, U., and I. Jackson (2005), The seismological signature of temperature and grain size variations in the upper mantle, *Earth Planet. Sci. Lett.*, *234*(1–2), 119–134, doi:10.1016/j.epsl.2005.02.008.

Fernandes, R., B. Ambrousius, R. Noomen, L. Bastos, L. Combrinck, J. Miranda, and W. Spakman (2004), Angular velocities of Nubia and Somalia from continuous GPS data: Implications on present-day relative kinematics, *Earth Planet. Sci. Lett.*, *222*, 197–208, doi:10.1016/j.epsl.2004.02.008.

Furman, T. (2007), Geochemistry of East African Rift basalts: An overview, *J. Afr. Earth Sci.*, *48*(2–3), 147–160.

Furman, T., J. Bryce, B. Hanan, G. Yirgu, and D. Ayalew (2006), Heads and tails: 30 years of the Afar plume, in *The Structure and Evolution of the East African Rift System in the Afar Volcanic Province*, edited by G. Yirgu, C. J. Ebinger, and P. K. H. Maguire, *Geol. Soc. London Spec. Publ.*, *259*, 95–119.

Gani, N., M. Gani, and M. Abdelsalam (2007), Blue Nile incision on the Ethiopian Plateau: Pulsed plateau growth, Pliocene uplift, and hominin evolution, *GSA Today*, *17*(9), 4–11.

George, R., N. Rogers, and S. Kelley (1998), Earliest magmatism in Ethiopia: evidence for two mantle plumes in one continental flood basalt province, *Geology*, *26*, 923–926.

Goes, S., R. Govers, and P. Vacher (2000), Shallow mantle temperatures under Europe from *P* and *S* wave tomography, *J. Geophys. Res.*, *105*(B5), 11,153–11,169.

Grand, S. P. (2002), Mantle shear-wave tomography and the fate of subducted slabs, *R. Soc. London Philos. Trans., Ser. A*, *360*, 2475–2491.

Gregg, P., J. Lin, M. Behn, and L. Montesi (2007), Spreading rate dependence of gravity anomalies along oceanic transform faults, *Nature*, *448*, 183–187, doi:10.1038/nature05962.

Griffiths, R., and I. Campbell (1990), Stirring and structure in mantle starting plumes, *Earth Planet. Sci. Lett.*, *99*, 66–78.

Gurnis, M., J. Ritsema, H.-J. van Heijst, and S. Zhong (2000), Tonga slab deformation: The influence of a lower mantle upwelling on a slab in a young subduction zone, *Geophys. Res. Lett.*, *27*(16), 2373–2376.

Hammond, W., and E. Humphreys (2000), Upper mantle seismic wave velocity: effects of realistic partial melt geometries, *J. Geophys. Res.*, *105*(B5), 10,975–10,986.

Hayward, N., and C. Ebinger (1996), Variations in the along-axis segmentation of the Afar rift system, *Tectonics*, *15*, 244–257.

Hofmann, C., V. Courtillot, G. Feraud, P. Rochette, G. Yirgu, E. Ketefo, and R. Pik (1997), Timing of the Ethiopian flood basalt event and implications for plume birth and global change, *Nature*, *389*, 838–841.

Jordan, T. (1988), Structure and formation of the continental tectosphere, *J. Petrol.*, Special Lithosphere Issue, 11–37.

Karato, S. (1993), Importance of anelasticity in the interpretation of seismic tomography, *Geophys. Res. Lett.*, *20*(15), 1623–1626.

Kazmin, V., A. Shifferaw, and T. Balcha (1978), The Ethiopian basement: Stratigraphy and possible manner of evolution, *Int. J. Earth Sci.*, *67*, 531–546.

Keir, D., G. Stuart, A. Jackson, and A. Ayele (2006), Local earthquake magnitude scale and seismicity rate for the Ethiopian Rift, *Bull. Seismol. Soc. Am.*, *96*(6), 2221–2230.

Kelemen, P., and W. Holbrook (1995), Origin of thick high-velocity igneous crust along the U.S. East coast margin, *J. Geophys. Res.*, *100*, 10,077–10,094.

Kendall, J.-M., G. Stuart, C. Ebinger, I. Bastow, and D. Keir (2005), Magma assisted rifting in Ethiopia, *Nature*, *433*, 146–148.

Kendall, J.-M., S. Pilidou, D. Keir, I. Bastow, G. Stuart, and A. Ayele (2006), Mantle upwellings, melt migration and the rifting of Africa: Insights from seismic anisotropy, in *The Structure and Evolution of the East African Rift System in the Afar Volcanic Province*, edited by G. Yirgu, C. J. Ebinger, and P. K. H. Maguire, *Geol. Soc. London Spec. Publ.*, *259*, 271–293.

Kennett, B., and E. Engdahl (1991), Traveltimes from global earthquake location and phase identification, *Geophys. J. Int.*, *105*(2), 429–465.

Keranen, K., and S. Klemperer (2007), Discontinuous and diachronous evolution of the Main Ethiopian Rift: Implications for development of continental rifts, *Earth Planet. Sci. Lett.*, *265*, 96–111.

Keranen, K., S. Klemperer, R. Gloaguen, and EAGLE Working Group (2004), Three-dimensional seismic imaging of a protoridge axis in the main Ethiopian rift, *Geology*, *32*, 949–952.

Kieffer, B., et al. (2004), Flood and shield basalts from Ethiopia: Magmas from the African Superswell, *J. Petrol.*, *45*(4), 793–834.

King, S., and J. Ritsema (2000), African hot spot volcanism: Small-scale convection in the upper mantle beneath cratons, *Science*, *290*, 1137–1140.

Kuo, B., and D. Forsyth (1988), Gravity anomalies of the ridge-transform system in the South Atlantic between 31 and 34.5°S: Upwelling centers and variations in crustal thickness, *Mar. Geophys. Res.*, *10*(3), 205–232.

Li, C., R. Van der Hilst, R. Engdahl, and S. Burdick (2008), A new global model for *P* wave speed variations in Earth's mantle, *Geochem. Geophys. Geosyst.*, *9*, Q05018, doi:10.1029/2007GC001806.

Lithgow-Bertelloni, C., and P. Silver (1998), Dynamic topography, plate driving forces and the African superswell, *Nature*, *395*, 269–272.

Mackenzie, G., H. Thybo, and P. Maguire (2005), Crustal velocity structure across the Main Ethiopian Rift: Results from 2-dimensional wide-angle seismic modelling, *Geophys. J. Int.*, *162*, 994–1006, doi:10.1111/j.1365-246X.2005.02710.x.

Maguire, P., et al. (2006), Crustal structure of the northern Main Ethiopian Rift from the EAGLE controlled-source survey: A snapshot of incipient lithospheric break-up, in *The Structure and Evolution of the East African Rift System in the Afar Volcanic Province*, edited by G. Yirgu, C. J. Ebinger, and P. K. H. Maguire, *Geol. Soc. London Spec. Publ.*, *259*, 271–293.

Mohr, P. (1967), Major volcanotectonic lineament in the Ethiopian rift system, *Nature*, *213*, 664–665.

Mohr, P. (1983), Ethiopian flood basalt province, *Nature*, *303*, 577–584.

Montelli, R., G. Nolet, F. Dahlen, G. Masters, E. Engdahl, and S.-H. Hung (2004), Finite-frequency tomography reveals a variety of plumes in the mantle, *Science*, *303*, 338–343.

Montelli, R., G. Nolet, F. Dahlen, and G. Masters (2006), A catalogue of deep mantle plumes: new results from finite-frequency tomography, *Geochem. Geophys. Geosyst.*, *7*, Q11007, doi:10.1029/2006GC001248.

Ni, S., and D. Helmberger (2003), Ridge-like lower mantle structure beneath South Africa, *J. Geophys. Res.*, *108*(B2), 2094, doi:10.1029/2001JB001545.

Ni, S., E. Tan, M. Gurnis, and D. Helmberger (2002), Sharp Sides to the African Superplume, *Science*, *296*, 1850–1852, doi:10.1126/science.1070698.

Nichols, A., M. Carroll, and Á. Höskuldsson (2002), Is the Iceland hot spot also wet? Evidence from the water contents of undegassed submarine and subglacial pillow basalts, *Earth Planet. Sci. Lett.*, *202*(1), 77–87.

Nyblade, A., and C. Langston (2002), Broadband seismic experiments probe the East African rift, *Eos Trans. AGU*, *83*, 405–410.

Nyblade, A., R. Knox, and H. Gurrola (2000), Mantle transition zone thickness beneath Afar: implications for the origin of the Afar hotspot, *Geophys. J. Int.*, *142*, 615–619.

Phipps-Morgan, J., and J. Chen (1993), Dependence of ridge–axis morphology on magma supply and spreading rate, *Nature*, *364*, 706–708.

Pik, R., C. Deniel, C. Coulon, G. Yirgu, and B. Marty (1999), Isotopic and trace element signatures of Ethiopian flood basalts: Evidence for plume-lithosphere interactions, *Geochem. Cosmochim. Acta*, *63*(15), 2263–2279.

Pik, R., B. Marty, J. Carignan, and J. Lavé (2003), Stability of the Upper Nile drainage network (Ethiopia) deduced from (U-Th)/He thermochronometry: Implications for uplift and erosion of the Afar plume dome, *Earth Planet. Sci. Lett.*, *215*, 73–88.

Pik, R., B. Marty, and D. Hilton (2006), How many mantle plumes in Africa? the geochemical point of view, *Chem. Geol.*, *226*(3–4), 100–114.

Poupinet, G. (1979), On the relation between *P*-wave travel time residuals and the age of the continental plates, *Earth Planet. Sci. Lett.*, *43*, 149–161.

Purcell, P. (1976), The Marda fault zone, Ethiopia, *Nature*, *261*, 569–571.

Ritsema, J., and R. Allen (2003), The elusive mantle plume, *Earth Planet. Sci. Lett.*, *207*, 1–12.

Ritsema, J., A. Nyblade, T. Owens, C. Langston, and J. VanDecar (1998), Upper mantle seismic velocity structure beneath Tanzania, East Africa: implications for the stability of cratonic lithosphere, *J. Geophys. Res.*, *103*(B9), 21,201–21,213.

Rogers, N. (2006), Basaltic magmatism and the geodynamics of the East African Rift System, in *The Structure and Evolution of the East African Rift System in the Afar Volcanic Province*, edited by G. Yirgu, C. J. Ebinger, and P. K. H. Maguire, *Geol. Soc. London Spec. Publ.*, *259*, 77–93.

Rogers, N., R. Macdonald, J. Fitton, R. George, R. Smith, and B. Barreiro (2000), Two mantle plumes beneath the East African rift system: Sr, Nd and Pb isotope evidence from Kenya Rift basalts, *Earth Planet. Sci. Lett.*, *176*, 387–400.

Rooney, T., T. Furman, G. Yirgu, and D. Ayalew (2005), Structure of the Ethiopian lithosphere: Xenolith evidence in the Main Ethiopian Rift, *Geochem. Cosmochim. Acta*, *69*(15), 3889–3910, doi:10.1016/j.gca.2005.03.043.

Rooney, T., T. Furman, I. Bastow, D. Ayalew, and G. Yirgu (2007), Lithospheric modification during crustal extension in the Main Ethiopian Rift, *J. Geophys. Res.*, *112*, B10201, doi:10.1029/2006JB004916.

Schilling, J., R. Kingsley, B. Hanan, and B. McCully (1992), Nd–Sr–Pb isotope variations along the Gulf of Aden: evidence for Afar mantle plume: Continental lithosphere interaction, *J. Geophys. Res.*, *97*, 10,927–10,966.

Simmons, N., A. Forte, and S. Grand (2007), Thermochemical structure and dynamics of the African superplume, *Geophys. Res. Lett.*, *34*, L02301, doi:10.1029/2006GL028009.

Stuart, G., I. Bastow, and C. Ebinger (2006), Crustal structure of the northern Main Ethiopian rift from reciever function studies, in *The Structure and Evolution of the East African Rift System in the Afar Volcanic Province*, edited by G. Yirgu, C. J. Ebinger, and P. K. H. Maguire, *Geol. Soc. London Spec. Publ.*, *259*, 271–293.

Tadesse, S., J.-P. Milesi, and Y. Deschamps (2003), Geology and mineral potential of Ethiopia: a note on geology and mineral map of Ethiopia, *J. Afr. Earth Sci.*, *36*, 273–313.

Tilmann, F., H. Benz, K. Priestley, and P. Okubo (2001), *P*-wave velocity structure of the uppermost mantle beneath Hawaii from traveltime tomography, *Geophys. J. Int.*, *146*, 594–606.

Vail, J. (1983), Pan-African crustal accretion in north-east Africa, *J. Afr. Earth Sci.*, *1*, 285–294.

VanDecar, J., and R. Crosson (1990), Determination of teleseismic relative phase arrival times using multi-channel cross-correlation and least squares, *Bull. Seismol. Soc. Am.*, *80*(1), 150–169.

VanDecar, J., D. James, and M. Assumpção (1995), Seismic evidence for a fossil mantle plume beneath South America and implications for plate driving forces, *Nature*, *378*, 25–31.

Vauchez, A., G. Barruol, and A. Tommasi (1997), Why do continents break-up parallel to ancient orogenic belts?, *Terra Nova*, *9*, 62–66.

Whaler, K., and S. Hautot (2006), The electrical resistivity structure of the crust beneath the northern Ethiopian rift, in *The Structure and Evolution of the East African Rift System in the Afar Volcanic Province*, edited by G. Yirgu, C. J. Ebinger, and P. K. H. Maguire, *Geol. Soc. London Spec. Publ.*, *256*, 293–305.

White, R., and D. McKenzie (1989), Magmatism at rift zones: The generation of volcanic continental margins and flood basalts, *J. Geophys. Res.*, *94*, 7685–7729.

WoldeGabriel, G. (1988), Volcanotectonic history of the central sector of the main Ethiopian rift: A geochronological, geochemical and petrological approach, Ph.D. thesis, Case Western Reserve Univ., Cleveland, Ohio.

WoldeGabriel, G., J. Aronson, and R. Walter (1990), Geology, geochronology, and rift basin development in the central sector of the Main Ethiopia Rift, *Bull. Geol. Soc. Am.*, *102*(4), 439–458.

Wolfenden, E., C. Ebinger, G. Yirgu, A. Deino, and D. Ayalew (2004), Evolution of the northern main Ethiopian rift: birth of a triple junction, *Earth Planet. Sci. Lett.*, *224*, 213–228.

Wright, T., C. Ebinger, J. Biggs, A. Ayele, G. Yirgu, D. Keir, and A. Stork (2006), Magma-maintained rift segmentation at continental rupture in the 2005 Afar dyking episode, *Nature*, *442*(7100), 291–294.

Yirgu, G., C. Ebinger, and P. Maguire (2006), The afar volcanic province within the East African Rift System: introduction, in *The Structure and Evolution of the East African Rift System in the Afar Volcanic Province*, edited by G. Yirgu, C. J. Ebinger, and P. K. H. Maguire, *Geol. Soc. London Spec. Publ.*, *259*, 1–6.